Available online at www.sciencedirect.com
ScienceDirect
ELSEVIER
Palaeogeography, Palaeoclimatology, Palaeoecology 243 (2007) 348–372
PALAEO
www.elsevier.com/locate/palaeo

Millennial-scale paleoclimate cycles recorded in widespread Palaeozoic deeper water rhythmites of North America

Maya Elrick [a,*], Linda A. Hinnov [b]

[a] Earth and Planetary Sciences, University of New Mexico, Albuquerque, New Mexico 87131, United States
[b] Earth and Planetary Sciences, Johns Hopkins University, Baltimore, Maryland 21218, United States

Received 27 March 2006; received in revised form 18 August 2006; accepted 23 August 2006

Abstract

Rhythmically interbedded limestone and shale or limestone and chert ("rhythmites") are a common feature of many deep-water Phanerozoic carbonate marine deposits. Seventeen different Palaeozoic rhythmite successions from across North America (8 studied in detail, 9 studied in reconnaissance) are described and summarized. Individual rhythmite couplets (4–20 cm thick) are composed of fine-grained, laminated to massive detrital limestone alternating with shale (or marl), or laminated spiculitic chert. Stratigraphic and primary depositional features within rhythmites and associated facies indicates that the carbonate-rich and carbonate-poor interbedding is the result of repetitive changes in sediment input (primary) rather than due to diagenetic redistribution of calcareous material (secondary).

The average duration of individual rhythmite couplets is calculated using spectral analysis (to determine couplet thickness) combined with biostratigraphically calibrated undecompacted average sediment accumulation rates. The duration of rhythmite couplets from the eight well studied successions ranges between ~150 and ~4900 yrs with the majority lying between ~1000 and 3000 yrs; i.e., millennial scale. The paucity and low diversity of skeletal and trace fossils, preserved suspension laminae, lack of sediment reworking, and facies associations indicate rhythmite accumulation was favored by: (1) deposition below storm-wave base which limited reworking by currents, (2) dysaerobic bottom waters which restricted bioturbation and intermixing of interbedded lithologies, and (3) proximity to nearshore carbonates supplying abundant fine-grained detrital carbonate. These combined conditions were best met along flooded, subtropical continental shelves or epeiric seas during My-scale (3rd-order) sea-level rises.

The rhythmic alternation between carbonate-rich and carbonate-poor layers is interpreted to represent millennial-scale paleoclimatic changes related to: (1) wet/dry climate cycles which influenced the amount of continent-derived eolian and/or fluvial sediment input, (2) variations in offshore transport (via storm-generated or density currents) of nearshore-derived terrigenous or carbonate sediments, and/or (3) changes in wind-driven upwelling and availability of recycled biogenic silica.

The various rhythmite successions accumulated under dramatically different paleoenvironment and paleogeographic conditions including active to passive tectonic settings, equatorial to subtropical latitudes, long-term icehouse through greenhouse climatic conditions, calcite versus aragonitic seas, variable atmospheric CO_2 concentrations, before and after land plant and animal evolution, and across widely varying ocean basin configurations.

If our short-term paleoclimatic interpretations for the rhythmites are correct, then it is apparent that millennial-scale climate changes occurred over a very wide spectrum of paleoceanographic, paleogeographic, paleoclimatic, tectonic, and biologic conditions and over time periods from the Cambrian to the Quaternary. Given this, it is difficult to invoke models of internally driven thermohaline oceanic oscillations or continental ice sheet instabilities to explain their origin. Instead, we suggest that

* Corresponding author.
E-mail address: dolomite@unm.edu (M. Elrick).

0031-0182/$ - see front matter
doi:10.1016/j.palaeo.2006.08.008

millennial-scale paleoclimate variability is a more permanent feature of the Earth's ocean–atmosphere system, which points to an external driver such as solar forcing.

Keywords: Millennial-scale climate change; Palaeozoic; Rhythmites; Carbonates

1. Introduction

Millennial-scale climate variability is a pervasive feature of many late Neogene–Quaternary marine, glacial, and terrestrial records, and occurs in deposits from polar to tropical latitudes, in the southern and northern hemispheres, and during glacial and interglacial times (e.g., Clark et al., 1999; Sarnthein et al., 2002). Although the temporal resolution of this climate signal varies depending on the system studied, the periods of late Neogene–Quaternary millennial-scale climate change cluster around ~1500 yrs and ~2500 yrs. Despite their ubiquitous nature, the origins of such climate change are still not understood.

While records of late Neogene–Quaternary millennial-scale climate variations are common, detection of similar scale oscillations in older paleoclimate archives is notably scarce. This is due in part to limitations in chronologic resolution, poorer preservation potential including the paucity of pre-Jurassic deep-sea sediments, and on a more basic level, to the difference in research focus of traditional sedimentary geologists versus paleoceanographers or paleoclimatologists. Despite these challenges, millennial-scale paleoclimate oscillations have been detected in some Mesozoic and Palaeozoic systems. The Permian Castile Formation of west Texas is composed of a remarkable ~250,000 yr-long evaporite succession with annual resolution recording prominent ~1500, ~1800, and ~2300 yr cycles (Anderson, 1982). Triassic deeper marine deposits from the southern Alps record ~2500–5000 yr cycles expressed as rhythmically interbedded limestone and shale couplets (Burchell et al., 1990). Limestone and marl couplets with durations of <3000 yrs are documented in Cambrian, Devonian, and Mississippian marine deposits from the western U.S. and are expressed as thin, rhythmically interbedded limestone and shale/marl layers or "rhythmites" (Elrick et al., 1991; Elrick and Hinnov, 1996). These Palaeozoic and Mesozoic examples provide intriguing insights into the origins of millennial-scale climate change because they developed under wide ranging palaeoenvironmental (climatic, oceanographic, tectonic, geographic, atmospheric, and biologic) conditions that were very different from those characterizing the past few million years of Earth history. Thus, the processes and conditions responsible for millennial-scale climate variability during the late Neogene–Quaternary are not unique and must have been operating at least as far back in time as the Cambrian.

Limestone–marl/shale rhythmites are known from all Phanerozoic time periods and accumulated within a wide range of depositional settings from shallow marine to hemipelagic, but are particularly common from deeper water settings of epeiric seas (e.g., Einsele and Ricken, 1991; Westphal and Munnecke, 2003). The origin of the visually striking rhythmicity between carbonate-rich and carbonate-poor layers is debated; many researchers believe the lithologic variations are due to cyclic fluctuations in depositional conditions (primary) which permits utilizing the rhythms for chronologic and paleoclimatic interpretations (e.g., Arthur et al., 1986). On the other hand, there are those who interpret the rhythmite development as strongly controlled by early (Munnecke and Samtleben, 1996) to late stage (Ricken, 1986) diagenetic redistribution of calcareous material (secondary); an interpretation which highlights the importance of diagenesis on carbonate facies.

The objectives of this paper are to: (1) review the persistent and widespread occurrence of Palaeozoic rhythmites across North America, (2) demonstrate their primary depositional origin at millennial time scales, (3) summarize the range of paleoenvironmental conditions that prevailed during rhythmite accumulation, and (4) briefly discuss the implications primary Palaeozoic rhythmites have on understanding the origin of pervasive late Neogene–Quaternary millennial-scale climate variability.

2. Palaeozoic rhythmite successions

A total of 17 different Palaeozoic rhythmite successions occurring across North America are presented in this study (Fig. 1); eight have been studied in detail (Table 1) and nine additional occurrences have been studied in reconnaissance (Table 2).

2.1. Lithologic and stratigraphic characteristics

Each rhythmite succession is characterized by thin, rhythmically interbedded, fine-grained limestone and

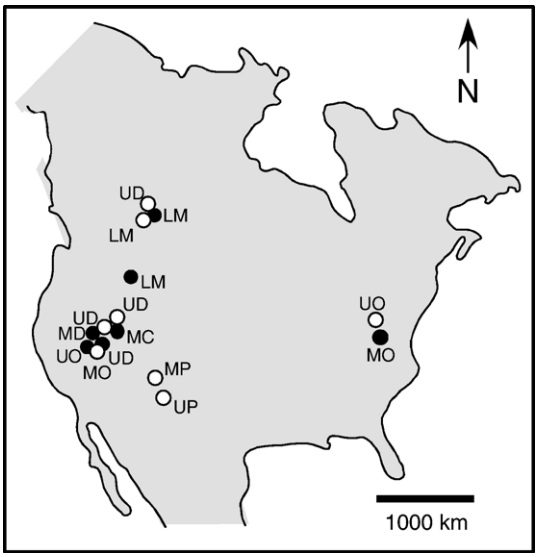

Fig. 1. Location of well studied (filled circles) and reconnaissance studied (open circles) rhythmite succession across North America. MC=Middle Cambrian Marjum Fm, MO=Middle Ordovician Liberty Hall Fm, UP=Upper Ordovician lower and upper Hanson Creek Fm, MD=Middle Devonian Denay Limestone, UD=Upper Devonian West Range Limestone, LM=Lower Mississippian Lodgepole and Banff Fms, MP=Middle Pennsylvanian Gobbler and Madera Fms, UP=Upper Permian Lamar Limestone.

marl or shale (Fig. 2). For brevity, limestone–marl (or shale) rhythmites are referred to as limestone–marl rhythmites regardless of the carbonate content of the carbonate-poor layer. The term marl is a descriptive term and refers to clayey or silty limestone and is not meant to imply a specific clay/silt concentration. Two of the rhythmite successions (upper Hanson Creek and Banff Formations) are unique in that they are composed of fine limestone interbedded with chert (Habib and Elrick, 2002) (Fig. 2F). Individual limestone and marl (or chert) layers are relatively constant in thickness (rather than nodular) and are laterally continuous over many tens to hundreds of meters. In addition, the rhythmite-bearing stratigraphic intervals (ten to hundreds of meters thick) can be correlated several to tens of km between isolated outcrops and in some cases, for over 500 km (Mississippian; Fig. 1).

Limestone layers are composed of laminated to massive, pelleted lime mudstone to lime mudstone (now microspar) and contain sparse to rare macrofossils (Fig. 3A). Marl layers are composed of laminated to massive, argillaceous to dolomitic pelletal lime mudstone and lime mudstone (Fig. 3B); shale layers range from mudshale to calcareous mudshale. Both marl and shales contain sparse to rare macrofossils, which are similar to types occurring in the associated limestones. Chert in the Upper Ordovician and Mississippian limestone–chert rhythmites is composed of dark, laminated to massive, calcareous spiculitic chert (Fig. 3C); early diagenetic dissolution and intra- and inter-layer redistribution of opaline silica resulted in the replacement of limestone by chert (Habib and Elrick, 2002).

Contacts between carbonate-rich and carbonate-poor layers are sharp to gradational (over <1 cm) (Figs. 1 and 3); sharp contacts are likely the result of pressure solution. Insoluble residues in marl layers range from 3 to 70 weight percent (wt.%) and are composed of clay (dominately illite), quartz silt, and organic matter. Insoluble residues in limestone layers range from 3 to 55 wt.% and are similar in composition to that in associated marl layers. Total organic carbon (TOC) values in marl layers range from below detection limits (<0.2 wt.%) to average values of 0.7 wt.% (with rare samples of 2.5 wt.%). Limestone TOC values range from below detection limits to 0.8 wt.%.

2.2. Depositional versus diagenetic rhythmites

In the diagenetic model of rhythmite development (Munnecke and Samtleben, 1996; Westphal et al., 2000), unstable aragonite is dissolved in the shallow-marine burial environment to form marl layers and is redistributed to adjacent layers as calcite cement to form limestone layers. This early cementation protects limestone layers from burial compaction, while the marl layers are highly compacted. Ricken (1986) suggested a similar model of carbonate dissolution and reprecipitation in the deep-burial environment. Some of the strongest evidence supporting a diagenetic origin for specific rhythmite successions within the sedimentary record includes: (1) primary depositional features (e.g., shell beds) cutting across limestone or marl layers, and (2) similiar ratios of diagenetically stable constituents (e.g., Ti/Al) and similar compositions or assemblages of diagenetically resistant organic-walled microfossils (palynomorphs) in carbonate-rich and carbonate-poor layers (e.g., Westphal et al., 2000, 2004).

The main evidence supporting a depositional origin for the Palaeozoic rhythmites of this study is the occurrence of primary depositional features including: (1) submillimeter-thick graded laminae in marls whose organized grain-size variations would not be preserved if pervasive carbonate dissolution occurred (Figs. 2B and 3B), (2) marl laminae onlapping cm-scale depositional relief on adjacent limestone layers; neither the marl laminae nor the delicate limestone microtopography would be preserved if large-scale carbonate dissolution occurred (Fig. 3D), (3) burrows within marl layers filled

Table 1
Summary of age and paleoenvironmental conditions during well studied Paleozoic rhythmite development

Age–formation	Location–paleolatitude	Couplet lithology	Succession thickness, # of couplets	Depositional setting, systems tract	Tectonic setting	Long-term climate calcite vs. aragonite seas	Major biotic events	References
Middle Cambrian Marjum Fm (*Bolaspodella*)	House Range, western Utah ~5°N	Laminated pelletal lime mudstone and marl	~330 m ~6000	Substorm wave base, basinal TST	Passive margin	Green -house Transitional seas	pre-land plants and animals	1, 2, 3
Middle Ordovician Liberty Hall Fm (Mohawkian)	West Virginia ~25°S	Laminated pelletal lime mudstone and calc. shale	25^{+} m ~350	Substorm wave base, basinal TST	Foreland basin	Green -house Calcite seas	Pre-land plants and animals	1, 4
Upper Ordovician lower Hanson Creek Fm (Ashgillian)	Monitor Range, central Nevada ~10–15°N	Laminated pelletal lime mdst and calc. shale	~30 m ~150	Substorm wave base, basinal TST/MFZ	Passive margin	Brief icehouse Calcite seas	Just prior to mass extinction	5, 6
Upper Ordovician Upper Hanson Creek Fm (late Hirnantian)		Laminated pelletal lime mdst and spicular chert	~30 m ~200	Substorm wave base, basinal, coastal upwelling system (cooler waters) TST/MFZ			Immediately after mass extinction	7, 8
Middle Devonian Denay Lst (Eifelian)	N. Antelope Range, central Nevada ~25°S	Pelletal lime mdst and marl	~55 m ~1000	Substorm wave base, slope and basin TST/MFZ	Passive margin	Green -house Calcite seas	Post-land plants and animals	1, 9, 10
Upper Devonian West Range Lst (Frasnian–Famennian)	Cherry Creek Range, NC Nevada ~15°S	Pelletal lime mdst and marl	~35 m ~370	Substorm wave base, slope/basin TST	Transition to foreland basin	Transitional Transitional seas	Just after mass extinction	11
Lower Mississippian Lodgepole Fm (Tournaisian)	Bridger Range, SW Montana ~0–5°N	Pelletal lime mdst and marl	~80 m >500	Substorm wave basin, ramp slope TST/MFZ	Foreland basin	Transitional Transitional seas	Reef-building organisms absent	12, 13
Lower Mississippian Banff Fm (Tournaisian)	SW Rundle Mtn., SW Alberta, Canada ~5–10°N	Laminated pelletal lime mdst, and calc. shale	~8 m 54	Substorm wave base, basinal TST/MFZ	Foreland basin	Transitional Transitional seas	Reef-building organisms absent	14, 15

TST=transgressive systems tract, MFZ=maximum flooding zone.
1=Elrick and Hinnov (1996), 2=Rees (1986), 3=Elrick and Snider (2002), 4=Read (1980), 5=Finney et al. (1999), 6=Harris and Sheehan (1997), 7=Finney et al. (1997), 8=Pope and Steffen (2003), 9=Elrick (1995), 10=Elrick (1996), 11=Sandberg et al. (1989), 12=Elrick and Read (1991), 13=Elrick et al. (1991), 14=Richards et al. (1993), 15=Brandley and Krause (1997).

with limestone (Fig. 3E), burrows in limestone filled with marl, and vertical burrows cross-cutting limestone–marl contacts, and (4) discrete graded marl laminae encased within limestone layers (Fig. 3F); if marls were an insoluble byproduct of carbonate dissolution, individual marl laminae would not occur within limestone layers. Limestone–chert rhythmites are also interpreted as depositional rhythmites (rather than the concentrated silica preserved after carbonate dissolution) because chert layers have submillimeter-thick graded laminae similar to marl layers (Fig. 3C); again, such grain-size organization would not be preserved during extensive dissolution.

Several lines of stratigraphic evidence support a depositional origin for the rhythmites. The Cambrian Marjum and Mississippian Banff Formations rhythmite-bearing stratigraphic intervals are interbedded with 2–6 m-thick intervals of homogenous calcareous shale, which lack limestone interbeds (e.g., Elrick and Snider, 2002; their Fig. 10). These thicker shale intervals occur basin-wide and are indistinguishable from the shale interbeds of the closely associated rhythmites. Given the lithologic similarity and close stratigraphic relationships, it is unlikely that the thicker homogenous shale intervals are depositional while the immediately associated and lithologically similar shale interbeds are diagenetic.

Table 2
Summary of age and paleoenvironmental conditions of reconnaissance Paleozoic rhythmites

Age–formation	Location–paleolatitude	Couplet lithology, average couplet thickness	Succession thickness	Depositional setting	Tectonic setting	Long-term climate, calscite vs. aragonite seas	Major biotic events
Middle Cambrian Wheeler Shale (early Bolaspidella)	Drum Mtns., western Utah ~5°N	Laminated pelletal lime mudstone and marl ~5–10 cm	~10s m	Substorm wave base, basinal/slope	Fault-bound passive margin embayment	Green-house Transitional	Pre-land plants and animals
Middle Ordovician Antelope Valley Fm (Whiterockian)	Hot Creek Range, central Nevada ~10–15°N	Laminated fine limestone and marl ~10 cm	<10 m	Substorm wave base, basinal/slope	Passive margin	Green-house Calcite	Pre-land plants and animals
Upper Ordovician Salona Formation (Caradocian)	State College, central Pennsylvania ~25°S	Laminated fine limestone and marl ~10–15 cm	~10s m	Substorm wave base, basinal	Foreland basin	Brief icehouse Calcite	Pre-land plants and animals
Upper Devonian Guilmette Fm/Devils Gate Lst (Frasnian–Famennian)	Devils Gate, central Nevada, ~20°S	Pelletal lime mdst. and calc. silststone/marl ~5–10 cm	<15 m	Substorm wave base, slope/basinal	Transitional to foreland basin	Transitional Calcite	Just prior and post mass extinction
Upper Devonian Mtn Hawk–Perdrix Fms (Frasnian)	Jasper area, W. Alberta, Canada 0–5°N	Fine limestone and calc. shale ~5–10 cm	~10s m	Substorm wave base, down slope of carbonate reefs	Active margin, foreland basin	Transitional Transitional	Just prior to mass extinction
Upper Devonian Pilot Shale (Frasnian–Famennian)	Coyote Knolls, western Utah ~20°S	Fine argillaceous limestone and marl ~10–20 cm	~10 m	Substorm wave basin, slope	Back-bulge of foreland basin system	Transitional Transitional	Just prior to mass extinction
Lower Mississippian Banff Fm (Tournaisian)	Mnt Chester, western Alberta ~5–10°S	Laminated fine limestone and chert ~10–20 cm	~10 m	Substorm wave base–upwelling system, basinal	Foreland basin	Transitional Transitional	Reef-building organisms absent
Middle Pennsylvanian Gobbler Fm and Madera Fm (Desmoinesian)	Sandia and Sacramento Mtns., New Mexico 0–5°	Pelletal lime mudstone and marl ~10–20 cm	<10 m	Substorm wave basin, deep ramp	Ancestral Rockies cratonic basin	Icehouse Aragonite	Reef-building organisms absent
Upper Permian Lamar Lst (Guadalupian)	West Texas ~5° N	Laminated fine limestone and silty limestone ~10–20 cm	10s m	Substorm wave base, slope/basin	Ancestral Rockies cratonic basin	Transitional Aragonite	None

Alternatively, using the diagenetic model, it might be argued, that the homogeneous calcareous shale interval lacked sufficient primary aragonite to promote the development of limestone interbeds and a subsequent increase in aragonite generated the overlying limestone–marl couplets.

The Cambrian, Middle Devonian, and Mississippian Lodgepole rhythmite successions are interbedded with debris flow and graded storm bed deposits (Elrick et al., 1991; Elrick and Snider, 2002). The Devonian debris flows are composed of reworked and folded rhythmite limestone clasts with a marl matrix (Fig. 4A); this indicates that the two lithologies existed on or very close to the seafloor and were incorporated into the debris flow. If the two lithologies were the product of diagenesis, they would not be available for incorporation into the episodic debris flows. Some of the rhythmites associated with the debris flows display soft-sediment folding related to debris flow emplacement (Fig. 4B); this indicates that both the limestone and marl layers were present immediately below the seafloor as distinct layers and were folded as the debris flow was emplaced. The Mississippian and Cambrian storm deposits are composed of 2–15 cm-thick layers of graded to wave-rippled skeletal limestones, which are conformably draped by laminated marls. The marl drapes indicate the availability of clay-rich material after waning storm conditions and are interpreted to represent final suspension settling after the storm passed. If the marl were product of diagenesis, it would not be available as loose material for deposition as mud drapes, nor would the marls consistently occur only at the tops of storm beds.

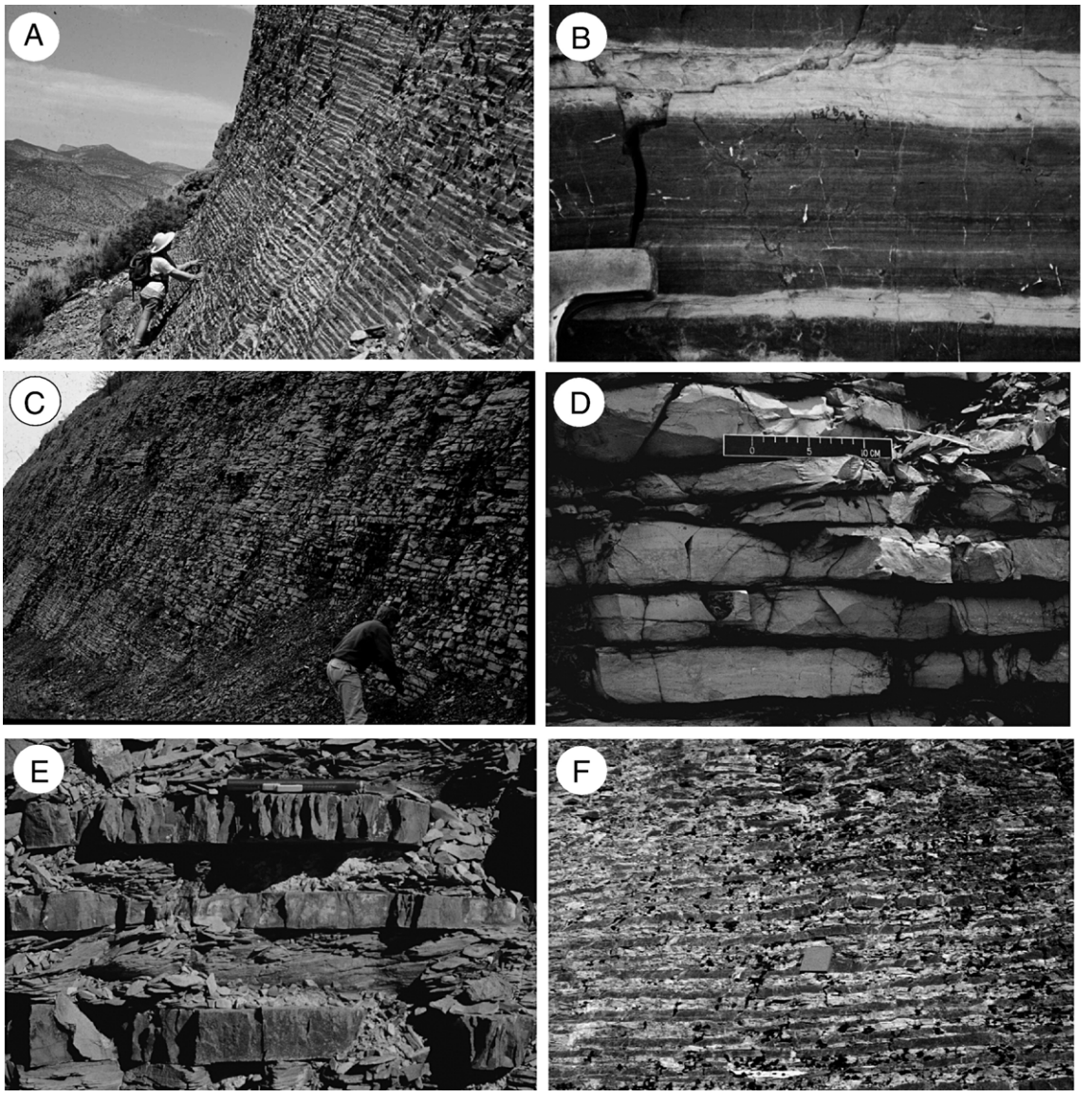

Fig. 2. Outcrop photographs of rhythmite successions. (A) Middle Cambrian Marjum Formation, western Utah. Limestone layers are dark gray, marls are light tan. (B) Close-up of Middle Cambrian rhythmites showing abundant suspension laminae in both limestone (dark gray) and marl (tan) layers. Note the gradational to sharp contacts. Hammer head for scale. (C) Middle Ordovician Liberty Hall Formation rhythmites from West Viriginia. (D) Close-up of Liberty Hall rhythmites showing interbedded limestones (light gray) and thin calcareous shale (black). (E) Close-up of Upper Ordovician lower Hanson Creek rhythmites from central Nevada showing dark limestone interbedded with thick calcareous shales. Pen for scale. (F) Upper Ordovician upper Hanson Creek limestone–chert rhythmites, central Nevada. Dark gray layers are limestone, light tan layers are chert layers which are dark gray/black on fresh surfaces. Field notebook for scale (20 cm).

The Cambrian, Upper Ordovician, and Upper Devonian rhythmite successions are conformably overlain by or interbedded with meter-scale intervals of nodular-bedded limestone–marl rhythmites followed by bioturbated argillaceous lime mudstones lacking limestone–marl interbedding. This gradational transition is interpreted to represent an increase in bottom-water oxygenation, which permitted increased infaunal bioturbation and homogenization of the rhythmite facies. This repeated and predictable succession of nodular to bioturbated intervals cannot be explained by the diagenetic model.

An additional line of evidence supporting a depositional origin for interbeds is the extensive lateral continuity and even thickness of individual layers (over hundreds of meters or more) and the persistence of specific rhythmite-bearing stratigraphic intervals over

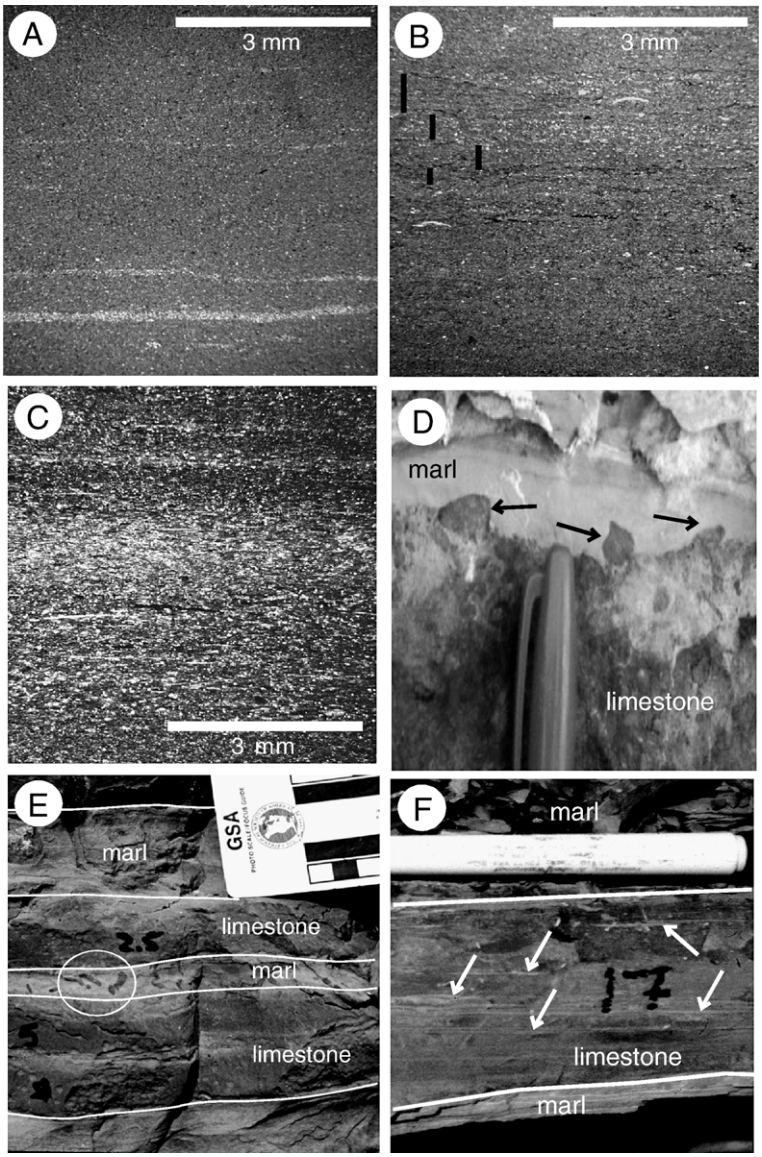

Fig. 3. Thin section (plane light) and field photographs of rhythmites. (A) Laminated limestone from the Lower Mississippian Banff Formation rhythmites showing typical texture of calcite microspar and submillimeter-thick laminae composed of coarser microspar crystals. (B) Laminated marl from the Middle Cambrian Marjum Formation composed of microspar, clay, rare agnostid trilobite fragments, and darker organic matter. Vertical black lines highlight size-graded laminae. (C) Laminated calcareous spiculitic chert from the Upper Ordovician upper Hanson Creek Formation showing abundant siliceous sponge spicules (elongate rods and circles), organic matter, and siliceous and calcareous matrix. Note well developed graded laminae. (D) Top of limestone layer (Middle Cambrian) with protruding unidentified steinkerns (black arrows) enclosed or onlapped by overlying light marl indicating marl layers are primary depositional features. Marker pen top for scale. (E) Upper Devonian West Range Limestone rhythmites with limestone-filled burrows (white circle) in marl layers indicating marl layers are primary. Cm-scale markers on ruler for scale. (F) Laminated limestone layer from the Lower Mississippian Banff Formation with arrows showing single marl laminae encased in limestone indicating marl is not a byproduct of carbonate dissolution. Marker pen for scale.

distances of tens to hundreds of km. These widespread occurrences preclude an origin related only to diagenesis because chemical gradients controlling cm-scale dissolution and solution transport would not likely remain consistent over such long distances.

Despite our depositional interpretation for the limestone–marl interbeds, we recognize in each studied example that differential diagenesis between limestone and marl layers has taken place because marl layers are significantly more compacted than limestone layers and

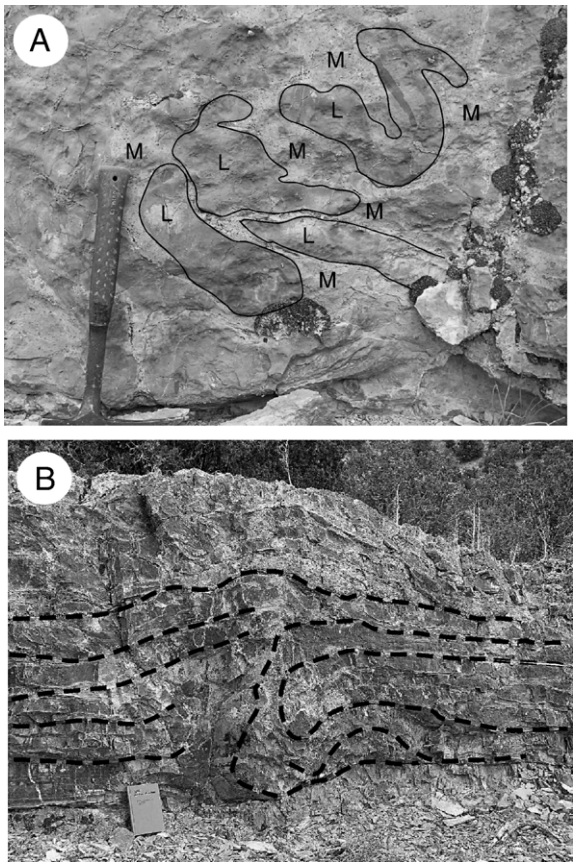

Fig. 4. Outcrop photographs of Middle Devonian Denay debris flow units and rhythmites. (A) Soft-sediment folding of limestone clasts within debris flow bed surrounded by marl matrix. Unconsolidated marl matrix must have been available on or very near the seafloor during debris flow emplacement. L=limestone clast, M=marl matrix; hammer handle for scale (B) Soft-sediment folding of limestone–marl rhythmites. Dotted lines trace particular marl layers involved in folding. Field notebook for scale in lower left (20 cm).

some amount of pressure solution has accentuated the sharpness of contacts between interbeds.

2.3. Rhythmite couplet periodicity

The average period (or duration) of individual limestone–marl or limestone–chert couplets within the eight well studied rhythmite successions was calculated using spectral analysis (to determine dominant couplet thickness) combined with biostratigraphically calibrated undecompacted average sediment accumulation rates (e.g., Elrick et al., 1991; Elrick and Hinnov, 1996). Rhythmite time series were originally generated from changes in weight percent (wt.%) $CaCO_3$. Wt.% $CaCO_3$ power spectra from Cambrian and Devonian rhythmites were then compared to spectra generated by numeric "ranking" of individual layers (limestone layers ranked as 2, marl layers ranked as 1) and were found to be essentially identical (Elrick and Hinnov, 1996); given these results, all subsequent spectral analysis were conducted using lithologic rank time series (Fig. 5A). Individual limestone and marl layers were measured to the nearest 4–5 mm; commonly layers less than 5 mm were not laterally continuous over 0.5–1 m, thus were not recorded as distinct layers. To test for "operator bias", two different geologists measured the thickness of interbeds along specific stratigraphic intervals within the Marjum and Liberty Hall rhythmites and spectral results were compared; the results between the comparisons were essentially identical.

The histograms and power spectra of these coded successions (Fig. 5B) give some common information, for example, the West Range Limestone histogram shows a highest percentage of couplets with 10 cm thickness; this is reflected by high power in the spectrum at the same wavelength. The spectra, however, provide a much expanded view of the couplet thickness distribution, and in addition, the spectral peaks additionally identify sequences of couplets with comparable thicknesses that occur with a regular pacing, whereas histograms record thicknesses regardless of their time-wise regularity.

Undecompacted average sediment accumulation rates for each of the well studied successions were calculated by measuring the thickness of biostratigraphically defined stratigraphic intervals, then tying the biostratigraphy into available numeric times scales to determine the average accumulation rates. It should be noted that the precision of typical Palaeozoic time intervals is quite poor and in many instances includes errors on the order of many millions of years. An example of our calculations is as follows: the stratigraphic thickness of the Lower Mississippian (specifically the Tournaisian as defined by conodont biostratigraphy) at the Banff rhythmite study locality is 490 m. The duration of the Tournaisian stage ranges from between 8 My and 13± 3.6 My depending on which geologic time scale is used (Ross and Ross, 1987; Harland et al., 1989; Fordam, 1992; Gradstein et al., 2004) (Table 3). The 490 m thickness was divided by the range of these Tournaisian durations to give a range of average sediment accumulation rates of between 2.8 and 6.1 cm/ky (Table 3). The total range of undecompacted average sediment accumulation rates for the eight rhythmite successions is between 1.9 and 21 cm/ky (Table 3).

The periods of couplets were determined by dividing the thickness of couplets (using the range of highest variance spectral peaks and median couplet thickness from couplet thickness histograms; Fig. 5A) by their

associated range of sediment accumulation rates. Using these methods, the eight well studied rhythmite successions range in duration from between ~147 and ~4910 yrs, with the majority lying between ~1000 and 3000 yrs (Fig. 5B; Table 3). Limitations on our time control do not permit us to detect frequency changes from one time period to another within the Palaeozoic.

The observed differential compaction between the marl and limestone layers of couplets means that time is unequally distributed within couplets; as a result, some of the peaks in the Palaeozoic spectra shown in Fig. 5B are likely generated by the distortion–compaction problem. Attempts at decompacting the marls relative to the limestones could reduce the "noise" within the spectra; we opt to illustrate unaltered spectral results to simply highlight the relatively uniform couplet thickness within each succession.

At present, there are no formal techniques for estimating spectral noise models for "binary" coded processes such as those represented by these series. Therefore, we have not attempted to assess the statistical significance of the various peaks in the estimated spectra beyond labeling dominant or well-defined ones. Bootstrap techniques may be useful for estimating noise (e.g., Efron and Tibshirani, 1993), although they are appropriate only for stationary series; i.e., series with stable frequency behaviour. As noted, sedimentation rates likely induce apparent frequency shifts in these data, thereby limiting the utility of bootstrap. However, this problem applies to all signal-to-noise estimation techniques applied to stratigraphic data. We anticipate addressing this estimation problem in future work on these and similar data.

We recognize that the undecompacted accumulation rates average rates over many millions of years and over varying facies, and include the effects of differential compaction, nondeposition, and erosion. However, even these simplified estimates generate accumulation rates which differ over an order of magnitude and still these indicate that the limestone–marl couplets represent less than a few thousand years of time.

Several lines of evidence unrelated to our accumulation rate estimates support the interpreted millennial-scale durations versus typical orbital-scale (~20–100 ky) durations. First, the number of successive couplets in any one Palaeozoic rhythmite succession ranges from over 50 to 6000. If the couplets are assumed to have a ~20 ky period (precessional), then the time span represented by the rhythmite-bearing intervals would be exceedingly long. For example, the ~6000 rhythmite couplets in the Middle Cambrian Marjum Formation would represent >100 My of time for a 400 m-thick stratigraphic interval spanning a single trilobite biozone within the Middle Cambrian (assuming Cambrian precessional periods of ~17.7 ky; Berger and Loutre, 1994). The Lower Mississippian Lodgepole Formation has over 500 successive couplets which would represent ~10 My of time for a small fraction of a single conodont biozone. Second, if a ~20 ky period is assumed for individual couplets, then average sediment accumulation rates would be <1 cm/ky, which is a rate more similar to modern open-ocean or abyssal plain rates and an order of magnitude lower than Holocene hemipelagic or inland sea rates (Enos, 1991). If 40 ky or 100 ky were assumed for the couplets (obliquity and eccentricity, respectively), the accumulation rates would slow accordingly. Such slow accumulation rates are unlikely considering that all of the rhythmites successions were deposited less than a few tens of km from their shallow-carbonate platform source areas. In addition, there is no sedimentologic evidence in any of the successions indicating slow sedimentation rates or condensed intervals (i.e., hardgrounds, highly burrowed intervals, concentration of authigenic minerals, or concentration and diverse faunal assemblages). In addition, limestone layers in the Lower Mississippian Lodgepole Formation rhythmites contain rare, in-growth position bryozoan fronds and rugose corals indicating relatively rapid sediment accumulation rates, essentially burying the organisms in their growth position. Such relationships would not occur if accumulation rates were on the order of a less than few cm/ky.

Fig. 5. (A) Lithologic rank time series of well studied rhythmites. Marl=1, limestone=2. (B) Spectral analysis of the well studied succession (left) and couplet thickness histograms (right). The spectra (solid line) of the rank series were calculated using the Blackman–Tukey estimator with 30% lags and Tukey windowing (Paillard et al., 1996). Dominant or well-defined spectral peaks are labeled in centimeters. Average sediment accumulation rates for each succession are shown in upper right (data for calculations in Table 3). Couplet thickness histograms were calculated using the field measurements of couplet thicknesses (to nearest 5 mm) with the exception of the Lower Mississippian Lodgepole data, and are displayed in 0.5 cm bins. Tables list basic statistics on couplet thickness data. Middle Cambrian Marjum Formation (length=904.7 cm; Δd=0.1 cm; bandwidth=0.004913 cycles/cm), Middle Ordovician Liberty Hall Formation (length=602.1 cm; Δd=0.1 cm; bandwidth=0.007383 cycles/cm), Middle Devonian Denay Formation (length=600.5 cm; Δd=0.1 cm; bandwidth=0.007403 cycles/cm), Upper Devonian West Range Limestone (length=565.5 cm; Δd=0.1 cm; bandwidth=0.007861 cycles/cm), Lower Mississippian Lodgepole Formation (length=3630.0 cm; Δd=0.1 cm; bandwidth=0.002453 cycles/cm), Lower Mississippian Banff Formation (length=736.5 cm; Δd=0.1 cm; bandwidth=0.006036 cycles/cm).

2.4. Depositional interpretations

Given the interpreted primary depositional origin and millennial-scale periods for the rhythmite couplets, it is obvious to ask what paleoenvironmental conditions oscillated on a repetitive basis to produce such persistent and rhythmic interbedding between the two contrasting lithologies. The paucity and low diversity of benthic

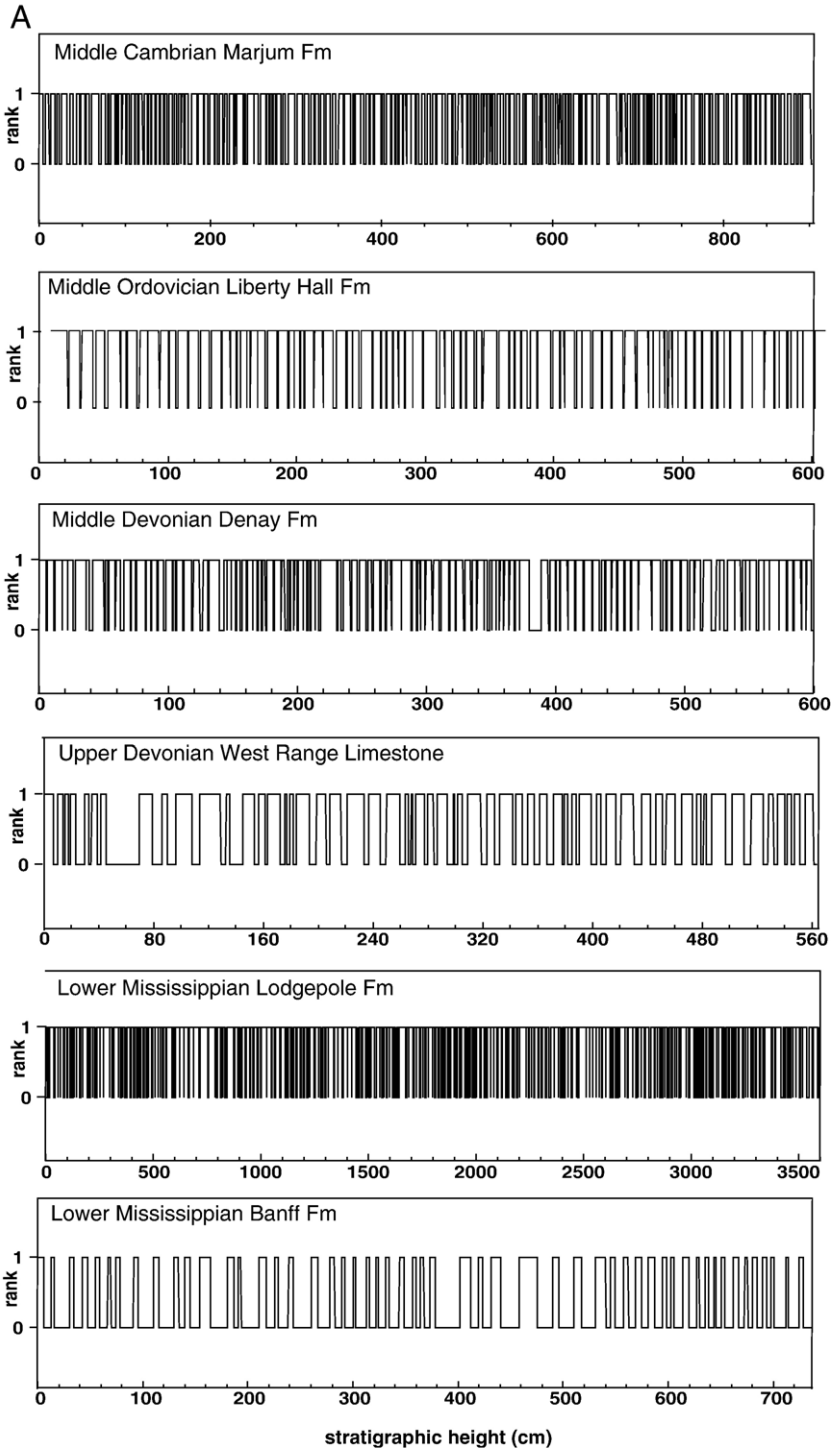

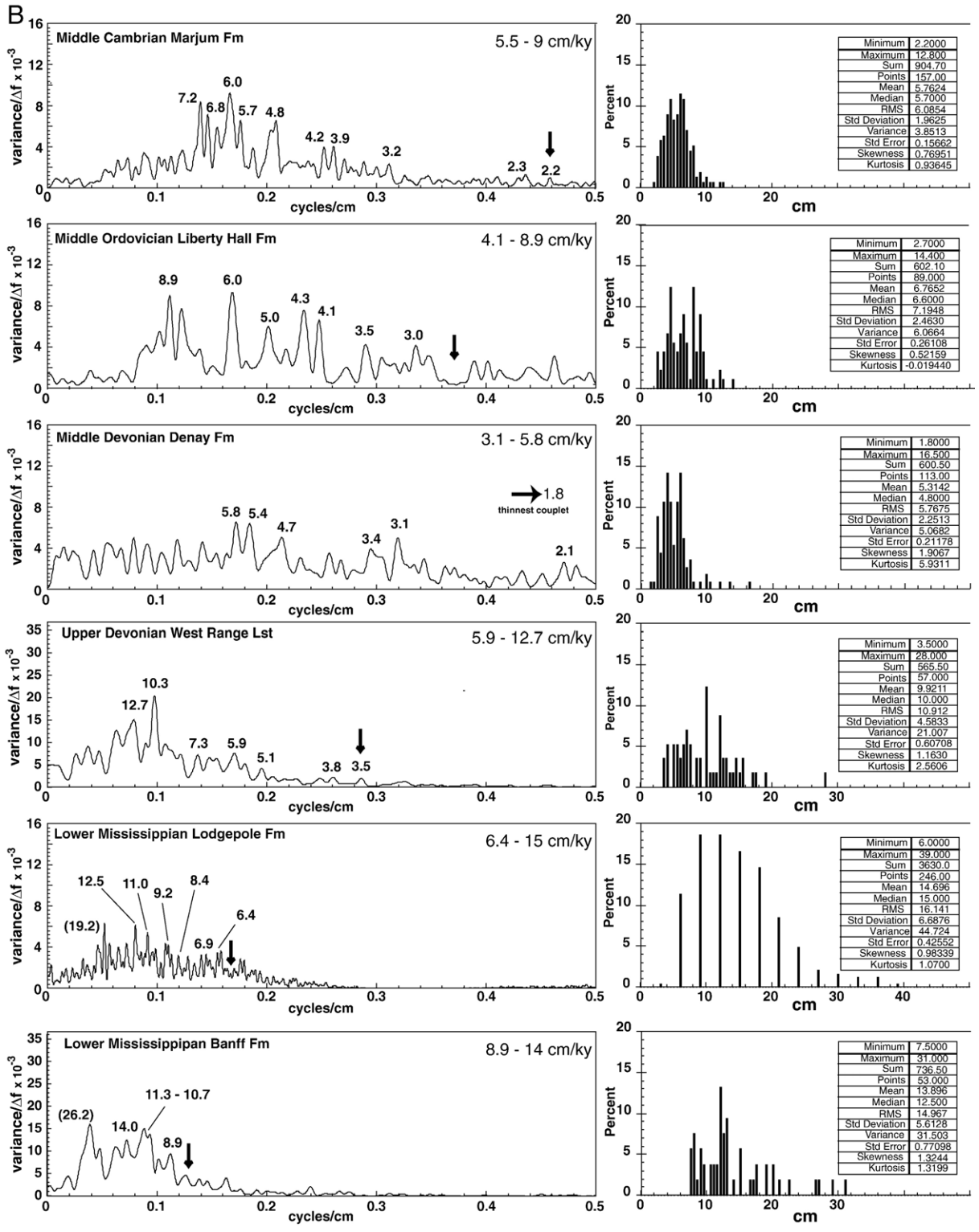

Fig. 5 (*continued*).

Table 3
Data used to calculate average sediment accumulation rates and couplet durations for 8 well studied rhythmite successions

Rhythmite succession	Biostratigraphic age and numeric duration★	Biostratigraphic interval thickness (m)◊	Average sediment accumulation rates (cm/ky)	Couplet thickness: spectral plots (cm)†,#	Couplet duration: spectral range (yrs)†,#
Middle Cambrian	Middle Cambrian (2)	815		4.8–7.2†	530–1700†
Marjum Fm	12±2.8 My (1)⊕		5.5–8.8	5.7#	630–1040#
	9 My (4,5)⊕		9		
Middle Ordovician	part Whiterockian	380	4.7	4.1–8.9†	1020–1530†
Liberty Hall Fm	and Mohawkian (7,8)			6.6#	1200#
	8 My (6)				
Upper Ordovician	Marysvillian and	235	4.3	19†	4410
lower Hanson Creek Fm	Richmondian (9)				
(limestone–marl)	5.5 My (6)				
Upper Hanson Creek Fm	Hirnantian (9, 18)	80	0–19.9	18∞	900–3390#
(limestone–chert)	1.9±2.12 My (1)				
	1.5 My (10)		5.3		
Middle Devonian	Eifelian and Givetian (3)	465			
Denay	9±13 My (11)		5.1–21	3.1–5.8	147–2000†
Limestone	11.5 My (12)⊕		5.3	4.8	228–1650#
	12.2±3.7 My (1)⊕		2.9–5.4		
	14 My (6)⊕		3.3		
Upper Devonian	Frasnian and	573			
West Range	Famennian (13)				968–3050†
Limestone	26.1±3.6 My (1)		1.9–2.5	5.9–12.7†	1500–2520#
	18 My (6)		3.2	10#	
	20.5 My (12)		2.8		
Lower Mississippian	Part Kinderkookian	195			
Lodgepole Fm	and Osagean (14, 17)				
	2.5 My (6)⊕		7.8	6.4–12.5†	820–1920†
	3 My (14)⊕		6.5	15#	1920–2300#
Banff Fm	Tournaisian (16)	490			
	13.9±3.2 My (1)		2.85–4.5	8.9–14†	1450–4910†
	13 My (11)		3.7	12.5#	2040–4380#
	9 My (6)		5.4		
	8 My (15)		6.1		

★References cited for numeric ages (uncertainties provided when reported) and biostratigraphy shown in parenthesis.
⊕Numeric ages based on most recent data and different from those reported in Elrick and Hinnov (1996) and Elrick et al. (1991).
◊Stratigraphic thicknesses measured at specific studied section.
†Range based on highest variance spectral peaks lying above 95% confidence interval in Fig. 4B.
#Median couplet thickness determined from histograms in Fig. 4B.
∞Average couplet thickness determined from number of couplets divided by rhythmite succession thickness.
1=Gradstein et al., 2004; 2=Robison, 1984; 3=Johnson et al., 1996; 4=Bowring and Erwin, 1998; 5=Young and Laurie, 1996; 6=Fordam, 1992; 7=Holland and Patzowsky, 1996; 8=Read, 1980; 9=Sweet, 2000; 10=Pope and Steffen, 2003; 11=Harland et al., 1989; 12=Tucker et al., 1998; 13=Sandberg et al., 1989; 14=Sando, 1985; 15=Ross and Ross, 1987; 16=Richards et al., 1993; 17=Sandberg and Gutschick, 1980, 18=Finney et al., 1997.

organisms (body and trace fossils), common preserved suspension laminae, lack of sedimentary structures indicative of current-reworking, and facies associations indicate that each rhythmite succession was deposited in quiet, dysaerobic bottom waters below storm-wave base. The similarity of features between the contrasting lithologies indicates that changes in water depth (sea-level change) were not directly involved in the development of the rhythmic interbedding. The Upper Ordovician limestone–chert rhythmites represent similar depositional settings within a regional coastal-upwelling zone, which affected western and southwestern North America during the Late Ordovician (Pope and Steffen, 2003).

Calcareous marine plankton (coccolithophores, pelagic foraminifera) supplying silt-size calcareous particles to the seafloor evolved in the early Mesozoic (Tappan and Loeblich, 1973). Thus, the fine calcareous particles in

these Palaeozoic rhythmites is interpreted to have been derived from the abrasion of coarser grained shallow-water carbonates and offshore transport by storm-generated or gravity flow currents; in other words, the limestone is detrital in origin. Supporting this detrital interpretation is that coeval deposits occurring farther offshore of the studied localities are commonly composed of shale or marl successions with either very thin limestone laminae or no interbedded limestone layers at all. This consistent decrease in limestone content in offshore directions suggests an onshore source for the limestone layers. Individual submillimeter-thick graded suspension laminae in both limestone and marl layers are interpreted to represent individual storm events or dilute density currents, with each limestone and marl layer containing several hundred events per layer. It is important to emphasize that individual limestone–marl couplets do not represent single events, rather they represent tens to hundreds of events.

Since both limestone and marl layers are composed of similar grain sizes (clay-through silt-size carbonate or silicate/siliceous particles), similar suspension laminae, and similar fossil types and abundances, we interpret similar depositional conditions during limestone and marl accumulation. The only difference between the carbonate-rich and carbonate-poor layers is the relative proportion of terrigenous silt and clay, or in the case of limestone–chert rhythmites, the relative proportion of siliceous sponge spicules. This observation implies that the transport mechanisms and dysaerobic bottom water conditions were maintained as each rhythmite succession accumulated with only the mineralogy (carbonate versus silicate) of the fine particles varying through time.

Determining whether detrital limestone or fine terrigenous material, or both, were fluctuating to produce the limestone–marl rhythmites is difficult. Previous workers have attempted various methods to distinguish which component was fluctuating including comparing variations in organic matter versus wt.% $CaCO_3$ (Ricken, 1991) or constructing plots of wt.% $CaCO_3$ versus Si/Al, P/Al, and Ba/Al ratios and ternary diagrams of Ca, Al, and organic matter (Arthur and Dean, 1991). Attempts at using these methods proved inconclusive for the studied Palaeozoic rhythmites. As a result, our interpretations leave open the possibility that one or both components were fluctuating through time.

2.5. Sediment sources and influx variations

Table 4 outlines the main sources and controls on fine terrigenous, detrital carbonate, and dissolved silica input into offshore marine basins at millennial time scales. The following brief discussion outlines the most reasonable mechanisms involved in Palaeozoic rhythmite development.

2.5.1. Terrigenous clay–silt

Continental-derived clay and silt is originally transported to marine shorelines by fluvial and/or eolian processes, then transported offshore by marine currents (storm-generated or gravity flow currents), delta progradation, or blown directly into the ocean by winds (Table 4). Controls on these eolian, fluvial, and marine transport processes can be grouped into tectonic (gravity flow currents, slope stability), climatic, and internally driven processes. Internally driven processes are those mechanisms which occur within the sedimentary system such as distributary channel avulsion and delta lobe migration, typical tidal flat progradation in response to onshore sediment accumulation, and simple bedform migration.

For the terrigenous component, we eliminate delta-lobe switching because it is unlikely that this could account for each Palaeozoic rhythmite occurrence as that would require each succession to be associated with a delta, and the delta would have to repeatedly switch at millennial time scales regardless of the paleoenvironmental/paleogeographic conditions associated with each succession (i.e., drainage basin size, fluvial discharge rates, shelf morphology, and associated marine currents). We discount a mechanism related to changes in vegetative cover because half of the studied successions accumulated before the evolution of terrestrial plants. Slope failure (tectonic or internally driven) is a common mechanism for the initiation of gravity flow currents. Using deep-water turbidities as earthquake proxies, Adams (1996), and Goldfinger et al. (2003) report that the average Holocene repeat time for rupture along major fault systems of the Cascadia subduction zone (convergent plate margin) and the northern San Andreas fault (transform plate margin) is on the order of ~600 yrs. While these recurrence intervals lie within the time range of the Palaeozoic rhythmites, it is unlikely that such recurrence intervals could be sustained for the 10^4–10^5 yr time spans of the rhythmite-bearing intervals and in the diverse tectonic settings represented by the various successions (see Tectonic Setting discussion).

The remaining controls on terrigenous influx are related to climate change (wind direction/intensity, source area aridity, precipitation, storm location/intensity/frequency, sea-level change, and flooding) (Table 4). Millennial-scale climate changes are documented throughout the late Neogene–Quaternary, and in particular, have been shown to affect eolian- and fluvial-derived terrigenous

Table 4
Possible sources and tectonic, climatic, and internally driven controls on accumulation of terrigenous, detrital carbonate, and dissolved silica into offshore marine basins

Lithology	Source and controls	
Terrigenous clay and silt	Eolian[c,i] Wind direction/intensity Source area aridity, vegetation Fluvial[c,i] Precipitation, vegetation Delta-lobe switching[i] Drainage basin characteristics, discharge, marine basin processes Marine transport Storm-generated currents Storm location, frequency, intensity Gravity flow currents[c,i,t] Seismicity, slope stability, sea level, floods	Marine transport[c] Storm-generated currents Storm location, frequency, intensity Gravity flow currents[c,i,t] Seismicity, slope stability, sea level, floods
Detrital carbonate	Nearshore carbonate productivity[c,i] Climate Temperature, salinity, storms, wave energy Ecology Evolution, nutrients, disease	
Chert (dissolved silica)	Continental silicate weathering[c,i] Soils, microbes, pH, vegetation, climate Submaine basalt hydrothermal alteration[i,t] Temperature, basalt thickness, alteration extent, eruption rates Upwelling[c] Wind direction/intensity, marine circulation	Offshore sponge spicule transport Storm-generated currents[c] Storm location, frequency, intensity Gravity flow currents[c,i,t] Seismicity, slope stability, sea level, floods

c = climate control, t = tectonic control, i = internally driven.

input into various shelf and deep-sea settings (e.g., Arz et al., 1998; Tada et al., 1999; Leuschner and Sirocko, 2000; Moreno et al., 2002).

2.5.2. Detrital carbonate

The fine detrital carbonate within carbonate-rich and carbonate-poor layers was originally produced within nearshore carbonate settings and was transported offshore by storm-generated or gravity flow currents. Millennial-scale variations in input to offshore basins were potentially controlled by changes in nearshore carbonate productivity or offshore marine transport, which are driven by internally driven, tectonic, and/or climatic processes (Table 4).

Short-term changes in nearshore carbonate productivity have been documented (e.g., Mallinson et al., 2003); however, they are linked to climate change influencing biologic productivity rather than internally driven (ecologic) factors. Even if short-term, ecologically driven changes were occurring to control the influx of detrital carbonate to offshore environments, it is not likely that such internally driven changes would be sustained over 10^4–10^5 yr time spans, nor would such consistent and repetitive changes be expected for each of the studied Palaeozoic time intervals. Seismic activity initiating slope failure and gravity flow currents are documented in the Holocene to occur at multi-centennial time scales (e.g., Adams, 1996); however, as argued

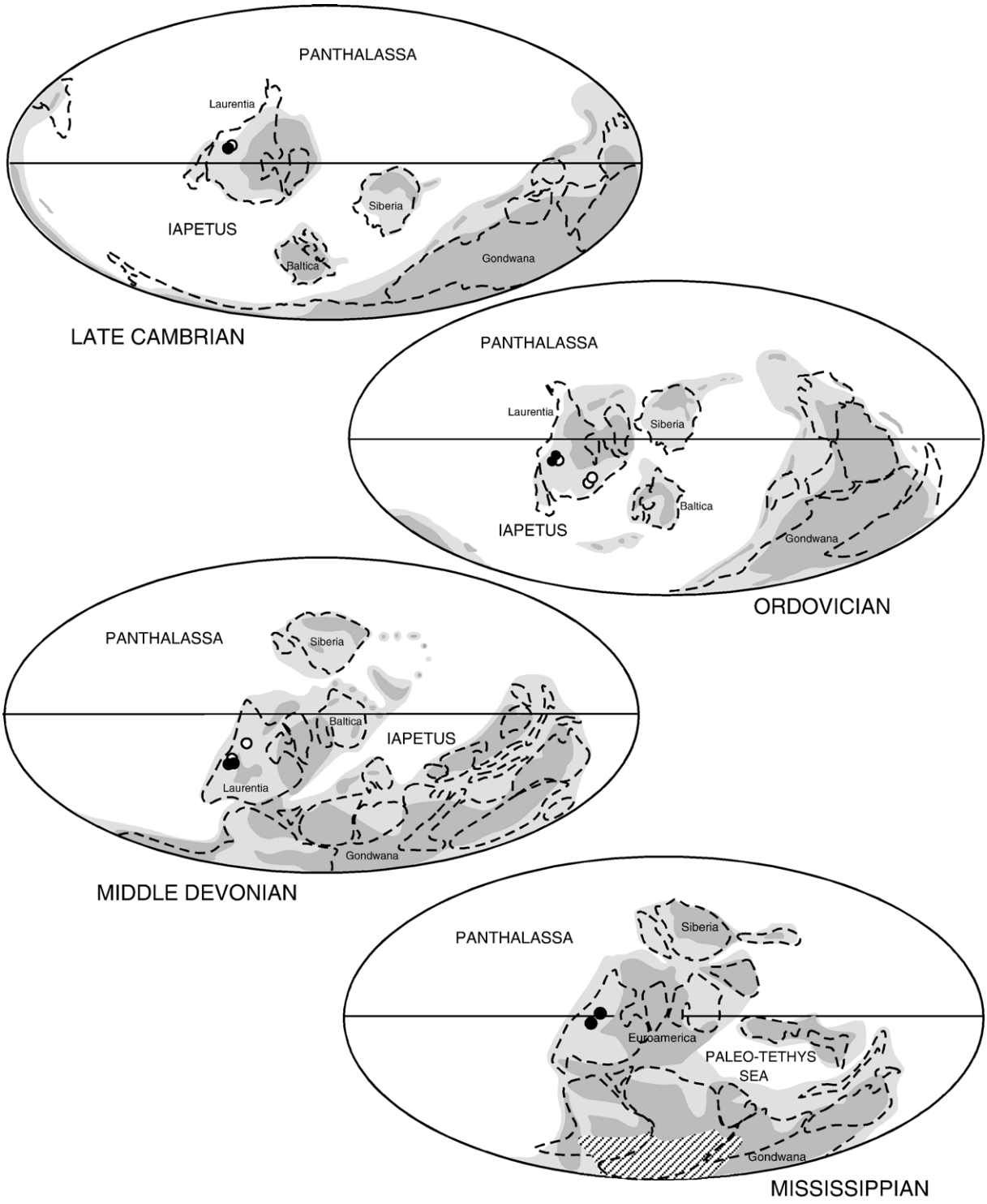

Fig. 6. Paleogeographic reconstructions of Palaeozoic rhythmite-bearing time intervals (modified from Scotese, 2001) showing wide spectrum of paleogeographic and paleoceanographic conditions during rhythmite development. Darker shading = exposed land masses, light shading = shallow marine environments, white = open ocean, diagonal lines = continental ice sheets. Filled circles show approximate locations of well studied rhythmite successions; unfilled circles show approximate locations of reconnaissance successions. Note that locations are approximations because the illustrated paleogeographic positions are time averaged over many millions of years and may not represent configurations at the specific time of rhythmite development.

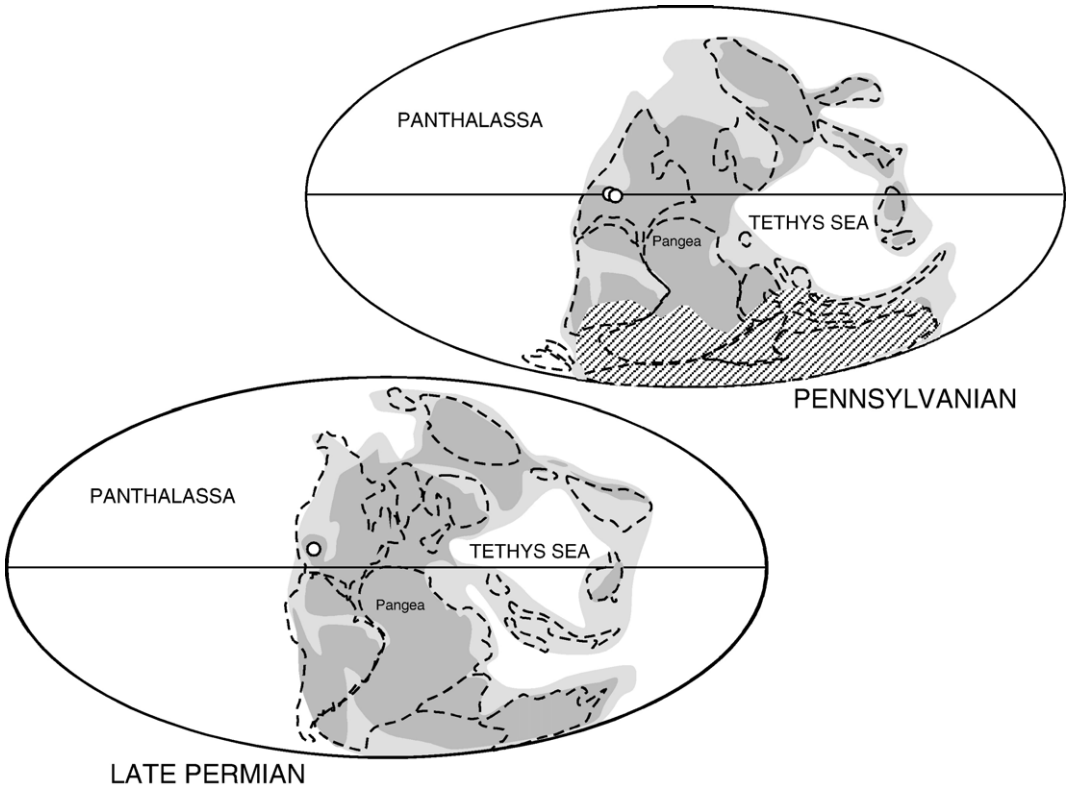

Fig. 6 (*continued*).

above, it is unlikely these recurrence intervals would occur in each of the studied successions, and be sustained over the 10^4–10^5 yr time spans of each rhythmite-bearing succession.

Short-term climate changes influencing nearshore carbonate productivity (via changes in temperature, salinity, turbidity, nutrient content, storm wave energy) and offshore transport have been documented in the Holocene (e.g., Greer and Swart, 2001; Mallinson et al., 2003) and provide a viable mechanism to explain the observed Palaeozoic trends.

2.5.3. Dissolved silica

The source for dissolved silica for the siliceous sponge spicules within chert layers was derived from (1) continental silicate weathering, (2) hydrothermal alteration of submarine basalts, and/or (3) coastal upwelling and recycling of dissolved biogenic silica (Table 4). Alternatively, the dissolved silica flux and sponge productivity could remain constant, while the offshore transport of disarticulated siliceous spicules by storm-generated or gravity flow currents could vary.

Short-term variations in continental weathering and hydrothermal-derived dissolved silica to offshore environments are influenced by various internally driven (vegetation, soil type/abundance, microbial activity, pH, basalt permeability and alteration extent) and climatically controlled (temperature, precipitation, pCO_2, fluvial discharge, marine circulation) processes (Table 4; Berner and Berner, 1997; Walther, 2005). We eliminate internal drivers because, as argued above, it is unlikely that the complex interplay of such processes could reoccur for each of the studied Palaeozoic time intervals and for sustained time spans.

Millennial-scale waxing and waning of mid-ocean ridge volcanism is reported for a segment of the East Pacific Rise (Cormeir et al., 2003). However, the pattern of associated hydrothermal circulation/alteration is controlled by differences in lava flow thickness and porosity, and fault density along ridge segments and it is unlikely that dissolved silica fluxes to shelf environments would mimic eruption rates and patterns. Short-term climate changes can control coastal upwelling patterns (wind direction/ intensity, seawater temperature, and sea-level), dissolved silica in fluvial discharge, and storm-generated currents. Recent examples of millennial-scale changes in upwelling (e.g., Piasis et al., 2001; Jung et al., 2002; Dupont et al., 2005),

fluvial sediment discharge (e.g., Tada et al., 1999; Moreno et al., 2002), and storminess (e.g., Noren et al., 2002) support a climatically controlled origin for the observed changes in Palaeozoic chert-limestone rhythmites.

In summary, the most reasonable mechanism for explaining the millennial-scale oscillations from carbonate-rich to carbonate-poor layers is short-term climate change. Although the specific mechanism is not clear, we suggest that the rhythmic alternations are the result of: (1) wet/dry climate cycles which influenced the amount of continent-derived eolian and/or fluvial sediment input, (2) variations in the offshore transport of nearshore terrigenous or carbonate sediments (i.e., storm-generated or density currents), and/or (3) changes in wind-driven upwelling and availability of recycled biogenic silica.

2.6. Paleoenvironmental conditions during rhythmite deposition

2.6.1. Paleogeographic and tectonic settings

The seventeen Palaeozoic rhythmite successions accumulated on both sides of the North American craton (Fig. 1) and were deposited across a range of subtropical to equatorial paleolatitudes (Fig. 6, Tables 1 and 2). The depositional basins formed along passive margins, fault-bound passive-margin embayments, forelands and back-bulge basins, or basins that developed during the transition from passive margins to foreland basins (Tables 1 and 2). Fig. 6 illustrates the wide range of paleogeographic configurations which existed during the development of each rhythmite succession and between the Palaeozoic and late Neogene–Quaternary configurations. For example, during the Cambrian and Ordovician, many continents were widely separated and extensively flooded, and North America straddled the paleoequator and was surrounded on all sides by oceans. By the Carboniferous and Permian, North America drifted into the northern hemisphere, the continents were widely exposed and assembled into Pangea, and the extensive Panthalassa and paleo-Tethys dominated the marine realm (Scotese, 2001). Of importance is not the exact location of accumulation of each rhythmite succession, rather that the location, size, and shape of the paleooceans were significantly different between each rhythmite time interval, as well as very different from late Neogene–Quaternary configurations. Given these widely varying paleogeographic and paleoceanographic conditions, it is apparent that the patterns and intensities of atmospheric circulation, heat and moisture transport, upwelling, and thermohaline circulation would vary greatly during each studied time interval and cannot be compared to those patterns which occurred over the last few million years.

2.6.2. Paleoclimatic and paleoceanographic settings

The Palaeozoic rhythmites were deposited during widely varying long-term (10s My) climatic and atmospheric regimes including: (1) greenhouse, icehouse, and transitional climate modes, (2) arid versus humid climate belts, and (3) varying atmospheric CO_2 concentrations (Fig. 7). Greenhouse climates are characterized by gentle pole-to-equator temperature gradients, high global sea levels and temperatures, and little evidence for significant continental ice sheets; icehouse climates are distinguished by the opposite trends (Fischer, 1984). Of the seventeen successions, six accumulated when the oceans were characterized as "calcite seas" (calcite being the dominant inorganic marine precipitate), two developed during times of "aragonite seas", and eight occurred during transitional times (Fig. 7) (Hardie, 1996; but see Westphal and Munnecke, 2003 for alternative interpretations). When the age of rhythmite successions are plotted against the 1st-order sea-level curve of Vail et al. (1977), they occur during all phases including long-term highs, lows, and transitional sea-level positions (Fig. 7). That lack of obvious relationships between these long-term boundary conditions and rhythmite occurrence suggests that rhythmite development was independent of these paleoenvironmental parameters. On the other hand, each of the studied successions accumulated during 3rd-

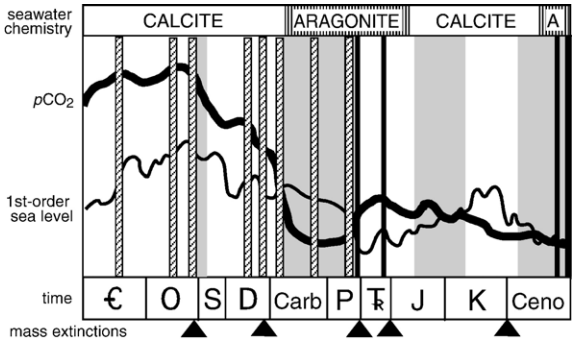

Fig. 7. Distribution of rhythmite successions with respect to geologic time, long-term climate (greenhouse=white, icehouse=gray shaded), 1st-order sea-level position (Vail et al., 1977), "calcitic seas" versus "aragonitic seas" (Hardie, 1996), atmospheric carbon dioxide content (Berner and Kothavala, 2001), and timing of major mass extinctions (Raup and Sepkoski, 1982). Bars with diagonal lines are Palaeozoic rhythmites from this study, solid black lines represent occurrences of previously reported millennial-scale records mentioned in text. Late Cenozoic solid black lines represent multiple late Neogene to Quaternary records which are too numerous to show individually.

order (~1–5 My) sea-level rises and form part of the transgressive systems tract (TST) or maximum flooding zone (MFZ). This can be predicted because maximum water depths (substorm wave base depths) would be attained during sea-level rises and shallow-water carbonate platforms would be flooded, carbonate productivity high, therefore offshore transport of detrital carbonate would be maximized (c.f., Schlager, 1993).

As rhythmites were developing along the outer shelf/offshore regions, nearshore environments were recording the effects of 10^4–10^5 yr (5th-order) sea-level fluctuations manifest by the occurrence of meter-scale, upward-shallowing carbonate cycles. For each of the well studied successions, the coeval nearshore 5th-order cycles have been previously interpreted as the result of glacio-eustatic, sea-level changes (Read, 1980; Bond et al., 1991; Elrick and Read, 1991; Montañez and Osleger, 1993; Elrick, 1995, 1996; LaMaskin and Elrick, 1997; Harris and Sheehan, 1997). This implies that during rhythmite formation, the shallow-water carbonate platforms were affected by 10^4–10^5 yr sea-level changes, yet these oscillations did not apparently affect the lithologic character or thicknesses of the coeval rhythmites. If the glacio-eustatic origin for the 5th-order cycles is correct, then this suggests that rhythmites formed throughout 5th-order sea-level rises (interglacial phases) and falls (glacial phases) without apparent change in character or thickness. Presently, it is not clear why the rhythmite successions lack overprinting by these 5th-order frequencies (orbital frequencies); however, rhythmites are observed at the base of some 5th-order Mississippian and Pennsylvanian cycles (c.f., Elrick et al., 1991) indicating they formed during the deepest water phase (interglacial) of cycle development.

2.6.3. Biologic evolution

The seventeen rhythmite successions occur over a total time span of ~250 My (Middle Cambrian to Late Permian) during which many significant evolutionary events occurred including two major global mass extinctions and associated re-radiations, and the inception of land animals and plants (Fig. 7). All of the rhythmites developed prior to the evolution of calcareous plankton (planktonic foraminifera, coccolithoporids) and when biogenic carbonate accumulation was restricted to continental margins and flooded cratons. The Cambrian and Ordovician rhythmites accumulated prior to the evolution of land plants and animals; thus prior to the time when continental weathering rates were influenced by complex relationships between vegetation and climate change. The two Upper Ordovician rhythmites successions accumulated immediately before and after the Late Ordovician mass extinction event and glaciation (Finney et al., 1999). Three of the Upper Devonian rhythmites accumulated immediately before and after the Late Devonian mass extinction (Sandberg et al., 1988). The occurrence of rhythmites closely associated with catastrophic changes in marine biota, including carbonate-secreting marine organisms, suggests that rhythmite development was not influenced by global changes in biologic diversity and abundance.

2.7. Discussion

Results from this study indicate that the relatively common occurrence of Palaeozoic deeper water rhythmites is favored by the following paleoenvironmental conditions: (1) deposition below storm-wave base to limit reworking by deeper marine currents, (2) dysaerobic bottom waters to restrict bioturbation and intermixing of interbedded lithologies, and (3) proximity to nearshore carbonates supplying abundant fine-grained detrital carbonate. These combined conditions were best met along flooded, subtropical continental shelves or epeiric seas during My-scale (3rd-order) sea-level rises.

Given these required conditions, it is not surprising that reports of late Neogene–Quaternary rhythmites are rare. In contrast to much of the Palaeozoic, sea levels during the last ~30–40 My have been low, and post-Eocene icehouse climate conditions resulted in abundant exposed continental margins, relatively narrow continental shelves, with thick nearshore carbonate accumulations restricted to relatively narrow latitudinal ranges (<35°N–S). In addition, the large amplitude, glacio-eustatic sea-level oscillations (and associated changes in wave base) characteristic of the past few million years resulted in extensive wave reworking of upper slope and shelf environments.

Despite these icehouse-related conditions, millennial-scale alternations in carbonate-rich versus carbonate-poor sedimentation are reported from Quaternary upper continental slope deposits off northeastern Brazil (Arz et al., 1998). Oxygen isotopes from planktonic foraminifera indicate that warming of surface waters coincided with more humid continental conditions and enhanced continental weathering, leading to increased terrigenous influx to the outer shelf and slope. During cooler phases and decreased continental weathering, more carbonate-rich deposits accumulated along the upper slope. Arz et al. (1998) relate the changes in surface-water temperatures and the resultant changes in continental humidity to variations in the intensity of the southeast trade winds.

Records of millennial-scale climate variability are well documented in early Pliocene through Holocene marine, terrestrial, and glacial records from both the northern and southern hemispheres, and from polar through to tropical latitudes. We cite examples from some of these settings below; additional examples are given by Alley et al. (1999), Leuschner and Sirocko (2000), Ruddiman (2001) and Sarnthein et al. (2002).

2.7.1. Glacial records

Denton and Stuiver (1967) and Denton and Karlen (1973) detected ~2000–3000 yr variations in the advance and retreat patterns of late Pleistocene–Holocene alpine glaciers in North America and Europe. More recently, glacial moraine and pollen studies in the Andes and New Zealand Alps reveal synchronous millennial-scale cooling and warming patterns, which correlate with those observed in the Northern Hemisphere ice record suggesting similar interhemispheric climate changes (Heusser et al., 1999; Denton et al., 1999). Some of the best known evidence for millennial-scale climate changes comes from long ice cores from the Greenland and Antarctica continental ice sheets which record ~1500 yr oscillations (Dansgaard–Oeschger cycles) in oxygen and hydrogen isotopes, and dust, salt, and methane concentrations (e.g., Yiou et al., 1991; Dansgaard et al., 1993; Grootes et al., 1993; Mayewski et al., 1994; Brook et al., 1996).

2.7.2. Marine records

Pleistocene to Holocene millennial-scale climate variability is documented in continental shelf, slope, and deep-sea sediments from around the globe. Within the North, South, and tropical Atlantic, abundant evidence for millennial-scale climate change is recorded in the $\delta^{18}O$ record of pelagic and benthic foraminifera (e.g., Curry and Oppo, 1997; Raymo et al., 1998; McManus et al., 1999), foraminifera assemblages (e.g., Little et al., 1997; Huls and Zahn, 2000), ice-rafted debris (IRD; Bond and Lotti, 1995), rock magnetic parameters (Moreno et al., 2002), carbonate percentage (Keigwin and Jones, 1994; Arz et al., 1998), and aragonite versus calcite abundances (Roth and Reijmer, 2005). Similar temporal variations are observed in the Indian Ocean by changes in dust abundance (Leuschner and Sirocko, 2000), laminated organic-rich sediments (Schulz et al., 1998), foraminifera assemblages (Reichart et al., 1998), and $\delta^{18}O$ record of foraminifera (Pestiaux et al., 1988). Within the Pacific Ocean, millennial-scale variations are observed in the abundance of IRD (Kotilainen and Shackleton, 1995), influx of glacial rock flour (Carter and Gammon, 2004), and the patterns of laminated versus bioturbated continental shelf deposits (Behl and Kennett, 1996). Foraminiferal $\delta^{18}O$ and $\delta^{13}C$ records of Southern Ocean sediments also suggest millennial-scale climate variability similar to that in the northern hemisphere, though they may lead in timing (Charles et al., 1996).

2.7.3. Terrestrial records

Millennial-scale climate oscillations are recognized in a wide variety of late Neogene–Quaternary terrestrial deposits. In middle to low latitude lake deposits of both hemispheres, this climatic signal is recorded by changes in eolian influx (De Decker et al., 1991) rainfall-, storm- and ENSO-induced sediment influx (e.g., Allen and Anderson, 1993; Noren et al., 2002; Moy et al., 2002), organic matter and lignite content (Steenbrink et al., 2003), pollen assemblages (Grimm, 1993), and $\delta^{18}O$ values, carbon content, and magnetic susceptibility (Benson et al., 1996). Short-term fluctuations have been identified in Chinese loess deposits indicated by changes in grain size, magnetic susceptibility, and carbonate content (Chen et al., 1996). In Europe, millennial-scale oscillations are observed by changes in soil character (Thouveny et al., 1994), pollen assemblages (Woillard and Mook, 1982), and spelothem stable isotopes (Wang et al., 2001; Genty et al., 2003). In western North America, fire-induced erosion and millennial-scale climate drought cycles are recorded in Holocene alluvial fan deposits (Meyer et al., 1995; Pierce et al., 2004), and a ~1500 yr rhythm is identified Holocene peat deposition in western interior Canada indicating regional wet–dry climate changes (Cambell et al., 2000).

It is beyond the scope of this paper to evaluate the mechanisms proposed to explain the origins of these late Neogene–Quaternary millennial-scale climate changes; however, the various hypotheses fall into the general categories of internal oscillations of the ocean–atmosphere system, periodic instabilities inherent to large ice sheets, and external forcing mechanisms. We briefly discuss these hypotheses to illustrate that paleoclimatologists focussed on the late Neogene–Quaternary commonly attribute millennial-scale climate changes to boundary conditions inherent to the late Cenozoic icehouse world and typically do not entertain pre-Cenozoic parameters.

Numerous modeling experiments report that centennial- to millennial-scale climate variability can be generated by internal oceanic processes which influence thermohaline circulation (THC) (e.g., Broecker et al., 1990; Sakai and Peltier, 1997; Winton, 1997; Paul and Schulz, 2002). The key element in each model is destabilization of a stratified high-latitude to polar water

column by diffusion/advection of warm subsurface waters, which rapidly increases THC. Stabilization of the water column is facilitated by freshwater/meltwater influx or an increase in poleward heat transport. Once THC or deep-water formation is reduced or shut down, the diffusion/advection stage repeats itself. Over the last several million years, the North Atlantic has been an important and sensitive region for deep-water formation because of its relatively elevated salinity, position with respect to freshwater/meltwater influx, and geographic/bathymetric configurations. In contrast, little deep-water formation is generated in the modern North Pacific because surface salinities in the Bering Sea are too low to create dense water, even after winter sea-ice formation (Kennett, 1982). These differences in deep-water formation in the modern North Pacific versus the North Atlantic illustrate how sensitive THC and its internal oscillations are to boundary conditions characteristic of the last few million years. While there is clear evidence from ocean modeling results that THC occurs over a wide range of ocean basin configurations, ice volumes, and pCO_2 concentrations (c.f., Huber and Sloan, 2001), it is difficult to image boundary-condition-sensitive THC variations would occur consecutively and uninterrupted many hundreds to thousands of times to generate the observed rhythmic interbedding.

It has been suggested that internal ice sheet instabilities result in ice surging followed by ice rafting at millennial time scales (MacAyeal, 1993). The resultant melt water influx affects sea-surface density, which strongly affects THC and potentially the global climate (Van Kreveld et al., 2000). The key elements in this model are the nature of the bedrock underlying the margins of continental ice sheets and the presence of ice sheets near areas of deep-water formation. This model may explain the rapid discharge of icebergs into the North Atlantic during the Pleistocene (Heinrich events); however, many of the Palaeozoic rhythmite successions accumulated during greenhouse climates when there is limited evidence of continental ice sheets, and in particular, little evidence for ice sheets adjacent to marine shorelines. While the effects of ice volume variability are inherently global in their ability to affect albedo, atmospheric and ocean circulation, nutrient supply/cycling, etc., it is unlikely that similar lithologic alternations would occur over such long time spans or as a result of such highly variable Palaeozoic global ice volume conditions.

Externally driven mechanisms include periodic climate forcing by variations in solar output (e.g., Van Geel et al., 1999; Bond et al., 2001) or long-period ocean tides (Keeling and Whorf, 2000). It has been argued that the Earth–Moon long-period tide with ~1800 yr duration might increase vertical mixing of seawater thereby causing episodic cooling of surface waters. The main argument against this model for explaining the observed Quaternary climate changes is that the ~1800 yr period is incompatible with the observed period of ~1470 yr (Schulz, 2002). Results from this study do not constrain the period of Palaeozoic rhythmites narrow enough to support or detract from the tidal model; in addition, the change in Earth–Moon distance since the Palaeozoic would have likely changed the long tidal cycle period.

Variations in solar activity as a mechanism to explain centennial- to millennial-scale climate change has been suggested for many decades (e.g., Bray, 1971; Suess, 1971; Eddy, 1976; Stuiver and Braziunas, 1989; Van Geel et al., 1999; Bond et al., 2001). The link between changes in solar output (as detected by covariations in the 14C and 10Be signal in tree rings and ice cores, respectively) and climate change has been detected in historical records (e.g., Eddy, 1976; Kilian et al., 1995) and in the Quaternary from varved lake deposits, IRD, sea surface temperatures, coarse sediment injections into the Norwegian Sea, and the GISP2 $\delta^{18}O$ record (Anderson, 1992; Finkel and Nishiizumi, 1997; Friedrich et al., 1999; Bond et al., 2001; Schulz and Paul, 2002; Sarnthein et al., 2003). Presently it is not clear how very small perturbations in solar radiation could be amplified within the climate system to generate the observed significant climate changes. Proposed mechanisms involve changes in UV radiation associated with variations in solar activity, followed by changes in stratospheric ozone production, which leads to atmospheric temperature and circulation variations (Haigh, 1996; Van Geel and Renssen, 1998). A second hypothesis suggests that variations in cosmic ray flux related to changes in solar activity influences cloudiness and atmospheric temperatures (Ney, 1959; Pudovkin and Raspopov, 1992; Svensmark and Friis-Christensen, 1997). If these ideas of solar forcing of Quaternary climates are correct, then it implies that the climate system is far more sensitive to small variations in solar activity than generally believed and it has major implications for understanding short-term climate changes observed in deep time.

If our interpretation for the origin of Palaeozoic rhythmites is correct, then it is apparent that millennial-scale climate changes occurred over a dramatic spectrum of oceanographic, geographic, climatic, tectonic, and biologic conditions and over time periods from the Cambrian to Quaternary. Given this, it is difficult to invoke models of internally driven THC oceanic oscillations or ice sheet instabilities to explain their origin.

Instead, we suggest that millennial-scale paleoclimate oscillations are a more permanent feature of the Earth's ocean–atmosphere system, which points to persistent external driver such as solar forcing.

Acknowledgements

Field assistance for this research was provided over the years by Katerina Petrontis, Matt Tremblay, Anna Snider, Mark Boslough, Peg Reese, Liz Langenberg, Mike Pope, and Jennifer Loomis. The manuscript benefited from the comments of Hildegard Westphal, Axel Munnecke, Finn Surlyk, and two anonymous reviewers.

References

Adams, J., 1996. Great earthquakes recorded by turbidites off the Washington–Oregon coast. Assessing earthquake hazards and reducing risk in the Pacific Northwest. U.S.G.S. Professional Paper 1560 (1), 147–158.

Allen, B.D., Anderson, R.Y., 1993. Evidence from western North America for rapid shifts in climate during the last glacial maximum. Science 260, 1920–1923.

Alley, R.B., Clark, P.U., Keigwin, L.D., Webb, R.S., 1999. Making sense of millennial-scale climate change: Part II: global impacts. In: Clark, P.U., Webb, P.S., Keigwin, L.D. (Eds.), Mechanisms of Global Climate Change at Millennial Time Scales. Geophysical Monograph, vol. 112, pp. 385–394.

Anderson, R.Y., 1982. A long geoclimatic record from the Permian. Journal of Geophysical Research 87, 7285–7294.

Anderson, R.Y., 1992. Possible connection between surface winds solar activity and Earth's magnetic field. Nature 359, 51–53.

Arthur, M.A., Dean, W.E., 1991. A holistic geochemical approach to cyclomania: examples from Cretaceous pelagic limestone sequences. In: Einsele, G., Ricken, W., Seilacher, A. (Eds.), Cycles and Events in Stratigraphy. Springer, Verlag, pp. 126–166.

Arthur, M.A., Bottjer, D.J., Dean, W.E., Fischer, A.J., Hattin, D.E., Dauffman, E.G., Pratt, L.M., Scholle, P.A., 1986. Rhythmic bedding in Upper Cretaceous pelagic carbonate sequences: varying sedimentary response to climate forcing. Geology 14, 153–156.

Arz, H.W., Pätzold, J., Wefer, G., 1998. Correlated millennial-scale changes in surface hydrography and terrigenous sediment yield inferred from last-glacial marine deposits of northeastern Brazil. Quaternary Research 50, 157–166.

Behl, R.J., Kennett, J.P., 1996. Brief interstadial events in the Santa Barbara basin, NE Pacific, during the past 60 kyr. Nature 379, 243–246.

Benson, L.V., Burdett, J.W., Kashgarian, M., Lund, S.P., Phillips, F.M., Rye, R.O., 1996. Climatic and hydrologic oscillations in the Owens Lake basin and adjacent Sierra Nevada, California. Science 274, 746–749.

Berner, R.A., Berner, E.K., 1997. Silicate weathering and climate. In: Ruddiman, W. (Ed.), Tectonic Uplift and Climate Change. Plenum Press, pp. 353–365.

Berner, R.A., Kothavala, Z., 2001. GEOCARB III: a revised model of atmospheric CO_2 over Phanerozoic time. American Journal of Science 301, 182–204.

Berger, A., Loutre, M.F., 1994. Astronomical forcing through geologic time. In: deBoer, P.L., Smith, D.G. (Eds.), Orbital Forcing and Cyclic Sequences. Special Publication, vol. 19. International Association of Sedimentologists, Blackwell Scientific, pp. 15–24.

Bond, G.C., Lotti, R., 1995. Iceberg discharges into the North Atlantic on millennial time scales during the last glaciation. Science 267, 1005–1010.

Bond, G.C., Kominz, M.A., Beavan, J., McManus, J., Bond, G.C., 1991. Are cyclic sediments periodic? Gamma analysis and spectral analysis of Newark Supergroup lacustrine strata. In: Watney, L., Franseen, E., Kendall, C., Ross, W. (Eds.), Sedimentary Modeling: Computer Simulations and Methods for Improved Parameter Definition. Kansas Geological Survey Bulletin, vol. 233, pp. 231–252.

Bond, G.C., Kromer, B., Beer, J., Muscheler, R., Evans, M., Showers, W., Hoffmann, S., Lotti-Bond, R., Hajdas, I., Bonani, G., 2001. Persistent solar influence on North Atlantic climate during the Holocene. Science 294, 2130–2136.

Bowring, S.A., Erwin, D.H., 1998. A new look at evolutionary rates in deep time: uniting a paleontology and high-precision geochronology. GSA Today 8, 1–8.

Brandley, R.T., Krause, F.F., 1997. Upwelling, thermoclines and wave-sweeping on an equatorial carbonate ramp: Lower Carboniferous strata of western Canada. In: James, N.P., Clarke, J.A.D. (Eds.), Cool-water Carbonates. SEPM Society for Sedimentary Geology Special Publication, vol. 56, pp. 365–390.

Bray, J.R., 1971. Solar–climate relationships in the post-Pleistocene. Science 171, 1242–1672.

Broecker, W.S., Bond, G., Klas, M., 1990. A salt oscillator in the glacial Atlantic: 1. The concept. Paleoceanography 5, 469–477.

Brook, E.J., Sowers, T., Orchardo, J., 1996. Rapid variations in atmospheric methane concentration during the past 110,000 years. Science 273, 1087–1091.

Burchell, M.T., Stefani, M., Masetti, D., 1990. Cyclic sedimentation in the Southern Alpine Rhaetic: the importance of climate and eustasy in controlling platform-basin interactions. Sedimentology 37, 795–815.

Cambell, I.D., Cambell, C., Yu, Z., Vitt, D.H., Apps, M.J., 2000. Millennial-scale rhythms in peatlands in the western interior of Canada and the global carbon cycle. Quaternary Research 54, 155–158.

Carter, R.M., Gammon, P., 2004. New Zealand maritime glaciation: millennial-scale southern climate change since 3.9 Ma. Science 304, 1659–1662.

Charles, C.D., Lynch-Steiglitz, J., Ninnemann, U.S., Fairbanks, R.G., 1996. Climate connections between the hemisphere revealed by deep-sea sediment core/ice core correlations. Earth and Planetary Science Letters 142, 19–27.

Chen, F.H., Bloemendal, J., Wang, J.M., Li, J.J., Oldfield, F., 1996. High-resolution multi-proxy climate records from Chinese loess: evidence for rapid climatic changes over the last 75 kyr. Palaeogeography, Palaeoclimatology, Palaeoecology 130, 323–335.

Clark, P.U., Webb, R.S., Keigwin, L.D., 1999. Mechanisms of global climate change at millennial time scales. Geophysical Monograph. American Geophysical Union, Wash. D.C., p. 112.

Cormeir, M., Ryan, W.B.F., Shah, A.K., Jin, W., Bradley, A.M., Yoerger, D.R., 2003. Waxing and waning volcanism along the East Pacific Rise on a millennium time scale. Geology 31, 633–636.

Curry, W.B., Oppo, D.W., 1997. Synchronous, high-frequency oscillations in tropical sea surface temperatures and North Atlantic deep water production during the last glacial cycle. Paleoceanography 12, 1–14.

Dansgaard, W., Johnson, S.J., Clausen, H.B., Dahl-Jensen, D., Gundestrup, N.S., Hammer, C.U., Hvidberg, C.S., Steffesen, J.P., Sveinbjornsdottir, A.E., Jouzel, J., Bond, G.C., 1993. Evidence for general instability of past climate from a 250-kyr ice-core record. Nature 364, 218–220.

De Decker, P., Correge, P., Head, J., 1991. Late Pleistocene record of cyclic eolian activity from tropical Australia suggesting the Younger Dryas is not an unusual climatic event. Geology 19, 602–605.

Denton, G.H., Karlen, W., 1973. Holocene climatic variations—their pattern and possible cause. Quaternary Research 3, 155–205.

Denton, G.H., Stuiver, M., 1967. Late Pleistocene glacial stratigraphy and chronology, northwestern Saint Elias Mountains, Yukon Territory, Canada. Geological Society of America Bulletin 78, 485–510.

Denton, G.H., Lowell, T.V., Heusser, C.J., Moreno, P.I., Andersen, B.G., Heusser, L.E., Schluchter, C., Marchant, D.R., 1999. Interhemispheric linkage of paleoclimate during the Last Glaciation. Glacial and Vegetational History of the Southern Lake, District of Chile. Geografkiska Annaler. Series A, Physical Geography, vol. 81, pp. 107–153.

Dupont, L.M., Donner, B., Vida, L., Perez, E.M., Wefer, G., 2005. Linking desert evolution and coastal upwelling; Pliocene climate change in Namibia. Geology 33, 461–464.

Eddy, J.A., 1976. The Maunder minimum. Science 193, 1189–1202.

Efron, B., Tibshirani, R.J., 1993. An Introduction to the Bootstrap. Chapman and Hall, London. 429 pp.

Einsele, G., Ricken, W., 1991. Limestone–marl alternations—an overview. In: Einsele, G., Ricken, W., Seilacher, A. (Eds.), Cycles and Events in Stratigraphy. Springer–Verlag, Berlin, pp. 23–47.

Elrick, M., 1995. Cyclostratigraphy of Middle Devonian carbonates of the eastern Great Basin. Journal of Sedimentary Research B65, 61–79.

Elrick, M., 1996. Sequence stratigraphy and platform evolution of Lower to Middle Devonian carbonates, eastern Great Basin. Geological Society of America Bulletin 108, 392–416.

Elrick, M., Hinnov, L.A., 1996. Millennial-scale climate origins for stratification in Cambrian and Devonian deep-water rhythmites, western USA. Palaeogeography, Palaeoclimatology, Palaeoecology 123, 353–372.

Elrick, M., Read, J.F., 1991. Cyclic ramp-to-basin carbonate deposits, Lower Mississippian, Wyoming and Montana: a combined field and computer modeling study. Journal of Sedimentary Petrology 61, 1194–1224.

Elrick, M., Snider, A.S., 2002. Deep-water stratigraphic cyclicity and carbonate mud mound development in the Middle Cambrian Marjum Formation, House Range, Utah, USA. Sedimentology 49, 1021–1047.

Elrick, M., Read, J.F., Coruh, C., 1991. Short-term paleoclimatic fluctuations expressed in Lower Mississippian ramp-slope deposits, southwestern Montana. Geology 19, 799–802.

Enos, P., 1991. Sedimentary parameters for computer modelling. In: Franseen, E.K., Watney, W.L., Kendall, C.G.St.C., Ross, W. (Eds.), Sedimentary Modeling: Computer Simulations and Methods for Improved Parameter Definition. Kansas Geological Survey Bulletin, vol. 233, pp. 63–100.

Fischer, A.G., 1984. The two Phanerozoic supercycles. In Catastrophes and Earth History; the new uniformitarianism. In: Berggren, W.A., Van Couvering, J.A. (Eds.), Princeton University Press, pp. 129–150.

Finkel, R.C., Nishiizumi, K., 1997. Beryllium 10 concentrations in the Greenland Ice Sheet Project 2 ice core from 3–40 ka. Journal of Geophysical Research 102 (C12), 26,669–26,706.

Finney, S.C., Cooper, J.D., Berry, W.B.N., 1997. Late Ordovician mass extinction: sedimentologic, cyclostratigraphic, and biostratigraphic records from platform and basin successions, central Nevada. Brigham Young University Geology Studies 42, 79–103.

Finney, S.C., Berry, W.B.N., Cooper, J.D., Ripperdan, R.L., Sweet, W.C., Jacobson, S.R., Soufiane, A., Achab, A., Noble, P.J., 1999. Late Ordovician mass extinction: a new perspective from stratigraphic sections in central Nevada. Geology 27, 215–218.

Fordam, B.G., 1992. Chronometric calibration of mid-Ordovician to Tournaisian conodont zones: a compilation from recent graphic correlation and isotope studies. Geological Magazine 129, 709–721.

Friedrich, M., Kromer, B., Spurk, M., Hofmann, J., Kaiser, K.F., 1999. Palaeo-environmental and radiocarbon calibration as derived from Late glacial/Early Holocene tree-ring chronologies. Quaternary International 61, 27–39.

Genty, D., Blarnart, D., Ouahdi, R., Gilmour, M., Bakder, A., Jouzel, J., Van-Exter, S., 2003. Precise dating of Dansgaard–Oeschger climate oscillations in western Europe from stalagmite data. Nature 421, 833–837.

Goldfinger, C., Nelson, C.H., Johnson, J.E., Shipboard Scientific Party, 2003. Deep-water turbidites as Holocene earthquake proxies: the Cascadia subduction zone and northern San Andreas fault systems. Annals of Geophysics 46, 1169–1194.

Gradstein, F.M., et al., 2004. A Geologic Time Scale. Cambridge University Press. 500 pp.

Greer, L., Swart, P.K., 2001. Changing patterns in Holocene precipitation as recorded by Dominican coral proxies. Abstracts with Programs - Geological Society of America 33, 158.

Grimm, E.C., 1993. A 50,000 year record of climate oscillations from Florida and its temporal correlation with the Heinrich events. Science 261, 198–200.

Grootes, P., Stuiver, M., White, J.W.C., Johnsen, S.J., Jouzel, J., 1993. Comparisons of oxygen isotope records from the GISP and GRIP Greenland ice cores. Nature 366, 552–554.

Habib, L., Elrick, M., 2002. Early silicification of Upper Ordovician deep-water chert–limestone rhythmites, central Nevada. Abstracts with Programs - Geological Society of America 17.

Haigh, J.D., 1996. The impact of solar variability on climate. Science 272, 981–984.

Hardie, L.A., 1996. Secular variation in seawater chemistry; an explanation for the coupled secular variation in the mineralogies of marine limestones and potash evaporites over the past 600 m.y. Geology 24, 279–283.

Harland, W.B., Armstrong, R.L., Cox, A.V., Craig, L.E., Smith, A.G., Smith, D.G., 1989. A Geologic Time Scale. Cambridge University Press, Cambridge, England. 263 pp.

Harris, M.T., Sheehan, P.M., 1997. Carbonate sequences and fossil communities from the Upper Ordovician–Lower Silurian of the eastern Great Basin. In: Link, P.K., Kowallis, B.J. (Eds.), Proterozoic to Recent Stratigraphy, Tectonics, and Volcanology, Utah, Nevada, southern Idaho and central Mexico. Brigham Young University Geology Studies, vol. 42, pp. 105–128.

Heusser, C.J., Heusser, L.E., Lowell, T.V., 1999. Paleoecology of the southern Chilean Lake District–Isla Grande de Chiloe during middle-late Llanquihue glaciation and deglaciation. Glacial and Vegetational History of the Southern, Lake District of Chile. Geografkiska Annaler. Series A, Physical Geography, vol. 81, pp. 231–284.

Holland, S.M., Patzowsky, M.E., 1996. Sequence stratigraphy and long-term paleoceanographic change in the Middle and Upper Ordovician of the eastern United States. Geological Society of America, Special Paper 306, 117–129.

Huber, M., Sloan, L.C., 2001. Heat transport, deep waters, and thermal gradients: coupled simulation of an Eocene greenhouse climate. Geophysical Research Letters 28, 3481–3484.

Huls, M., Zahn, R., 2000. Millennial-scale sea surface temperature variability in the western tropical North Atlantic from planktonic foraminiferal census counts. Paleoceaongraphy 15, 659–678.

Johnson, J.G., Klapper, G., Elrick, M., 1996. Devonian transgressive–regressive cycles and biostratigraphy, Northern Antelope Range, Nevada: establishment of reference horizons for global cycles. Palaios 11, 3–14.

Jung, S., Ivanova, E., Reichart, G.J., Davies, G.R., Ganssen, G., Kroon, D., van Hinte, J.E., 2002. Centennial–millennial-scale monsoon variations off Somalia over the last 35 ka. Geological Society Special Publication 195, 341–352.

Keeling, C.D., Whorf, T.P., 2000. The 1800-year oceanic tidal cycle: a possible cause of rapid climate change. Proceedings of the National Academy of Sciences of the United States of America 97, 3814–3819.

Keigwin, L.D., Jones, G.A., 1994. Western North Atlantic evidence for millennial-scale changes in ocean circulation and climate. Journal of Geophysical Research 99, 12,397–12,410.

Kennett, J.P., 1982. Marine Geology. Prentice Hall Inc., New Jersey. 813 pp.

Kilian, M.R., van der Plicht, J., van Geel, B., 1995. Dating raised bogs: aspects of AMS 14C wiggle matching, a reservoir effect and a climatic change. Quaternary Science Reviews 14, 959–966.

Kotilainen, A.T., Shackleton, N.J., 1995. Rapid climate variability in the North Pacific Ocean during the past 95,000 years. Nature 377, 323–326.

LaMaskin, T.A., Elrick, M., 1997. Sequence stratigraphy of the Middle to Upper Devonian Guilmette Formation, Southern Egan and Schell Creek Ranges, Nevada. In: Klapper, G., Murphy, M.A., Talent, J.A. (Eds.), Palaeozoic Sequence Stratigraphy, Biostratigraphy, and Biogeography: Studies in Honor of J. Granville "Jess" Johnson: Geological Society of America Special Paper, vol. 321, pp. 89–112.

Leuschner, D.C., Sirocko, F., 2000. The low-latitude monsoon climate during Dansgaard–Oeschger cycles and Heinrich events. Quaternary Science Reviews 19, 243–254.

Little, M.G., Schneider, R.R., Kroon, D., Price, B., Summerhayes, C.P., Segl, M., 1997. Trade wind forcing of upwelling, seasonality, and Heinrich events as a response to sub-Milankovitch climate variability. Paleoceanography 12, 568–576.

MacAyeal, D.R., 1993. Binge/purge oscillations of the Laurentide ice sheet as a cause of North Atlantic's Heinrich events. Paleoceanography 8, 775–784.

Mallinson, D.J., Hine, A.C., Hallock, P., Locker, S.D., Shinn, E.A., Naar, D.F., Donahue, B.T., Weaver, D., 2003. Development of small carbonate banks on the South Florida platform margin; response to sea level and climate change. Marine Geology 199, 45–63.

Mayewski, P.A., Meeker, L.D., Whitlow, S., Twickler, M.S., Morriso, M.C., Bloomfield, P., Bond, G.C., Alley, R.B., Gow, A.J., Grootes, P.M., Meese, D.A., Ram, M., Taylor, K.C., Wumkes, W., 1994. Changes in atmospheric circulation and ocean cover over the North Atlantic during the last 41,000 years. Science 263, 1747–1751.

McManus, J.F., Oppo, D.W., Cullen, J.L., 1999. A 0.5-million-year record of millennial-scale climate variability in the North Atlantic. Science 283, 971–975.

Meyer, G.A., Wells, S.G., Jull, A.J., 1995. Fire and alluvial chronology in Yellowstone National Park: climatic and intrinsic controls on Holocene geomorphic processes. Geological Society of America Bulletin 107, 1211–1230.

Montañez, I.P., Osleger, D.A., 1993. Parasequences stacking patterns, third-order accommodation events, and sequence stratigraphy of Middle to Upper Cambrian platform carbonates, Bonanza King Formation, southern Great Basin. In: Loucks, B., Sarg, J.F. (Eds.), Recent Advances and Applications of Carbonate Sequence Stratigraphy. American Association of Petroleum Geologists Memoir, vol. 57, pp. 305–326.

Moy, C.M., Seltzer, G.O., Rodbell, D.T., Anderson, D.M., 2002. Variability of El Nino/Southern Oscillation activity at millennial timescales during the Holocene epoch. Nature 420, 162–165.

Moreno, E., Thourveny, N., Delanghe, D., McCave, I., Shackleton, N.J., 2002. Climatic and oceanographic changes in the Northeast Atlantic reflected by magnetic properties of sediments deposited on the Portuguese margin during the last 340 ka. Earth and Planetary Science Letters 202, 465–480.

Munnecke, A., Samtleben, C., 1996. The formation of micritic limestones and the development of limestone–marl alternations in the Silurian of Gotland, Sweden. Facies 34, 159–176.

Ney, E.P., 1959. Cosmic radiation and the weather. Nature 183, 451–452.

Noren, A.J., Bierman, P.R., Steig, E.J., Andrea Lini, A., Southon, J., 2002. Millennial-scale storminess variability in the northeastern United States during the Holocene Epoch. Nature 419, 821–824.

Paillard, D., Labeyrie, L., Yiou, P., 1996. Macintosh program performs time-series analysis. Eos, Trans. - Am. Geophys. Union 77, 379.

Paul, A., Schulz, M., 2002. Holocene climate variability on centennial-to-millennial time scales: 2. Internal feedbacks and external forcings as possible causes. In: Wefer, G., Hehre, W.H., Jansen, E. (Eds.), Climate Development and History of the North Atlantic Realm. Springer–Verlag, pp. 55–73.

Pestiaux, P., Van der Mersch, I., Berger, A., Duplessy, J.C., 1988. Paleoclimate variability at frequencies ranging from 1 cycle per 10000 years to 1 cycle per 1000 years: evidence for non-linear behavior of the climate system. Climate Change 12, 9–37.

Piasis, N.G., Mix, A.C., Heusser, L., 2001. Millennial scale climate variability of the northeast Pacific Ocean and northwest North America based on radiolaria and pollen. Quaternary Science Reviews 20, 1561–1576.

Pierce, J.L., Meyer, G.M., Jull, T., 2004. Fire-induced erosion and millennial-scale climate change in northern ponderosa pine forests. Nature 432, 8790.

Pope, M.C., Steffen, J.B., 2003. Widespread, prolonged late Middle to Late Ordovician upwelling in North America: a proxy record of glaciation? Geology 31, 63–66.

Pudovkin, M.I., Raspopov, O.M., 1992. The mechanism of action of solar activity on the state of lower atmosphere and meteorological parameters. Geomagnetism and Aeromony English Ed. 325, 593–608.

Raup, D.H., Sepkoski, J., 1982. Mass extinctions in the fossil record. Science 215, 1501–1503.

Raymo, M.E., Ganley, K., Carter, S., Oppo, D.W., McManus, J., 1998. Millennial-scale climate instability during the early Pleistocene epoch. Nature 392, 699–702.

Read, J.F., 1980. Carbonate ramp-to-basin transitions and foreland basin evolution, Middle Ordovician, Virginia Appalachians. American Association of Petroleum Geologists Bulletin 64, 1575–1612.

Rees, M.N., 1986. A fault-controlled trough through a carbonate platform: the Middle Cambrian House Range embayment. Geological Society of America 97, 1054–1069.

Reichart, G.J., Lourens, L.J., Zachariasse, W.J., 1998. Temporal variability in the northern Arabian Sea Oxygen Minimum Zone OMZ during the last 224,000 years. Paleoceanography 13, 607–621.

Richards, B.C., Bamber, E.W., Higgins, A.C., Utting, J., 1993. Carboniferous; Subchapter 4E in Sedimentary Cover of the Craton in Canada. In: Stott, D.F., Aitken, J.D. (Eds.), Geological Survey of Canada. Geology of Canada, vol. 5, pp. 202–271.

Ricken, W., 1986. Diagenetic bedding: model for marl–limestone alternations. Lecture Notes in Earth Sciences, vol. 6. Springer, Berlin. 210 pp.

Ricken, W., 1991. Variation of sedimentation rates in rhythmically bedded sediments: distinction between depositional types. In: Einsele, G., Ricken, W., Seilacher, A. (Eds.), Cycles and Events in Stratigraphy. Springer–Verlag, pp. 166–187.

Robison, R.A., 1984. Cambrian Agnostida from North America and Greenland: Part 1, Ptychagnostidae. University of Kansas Paleontological Contributions. Papers 109, 28.

Ross, C.A., Ross, J.R.P., 1987. Late Paleozoic sea-levels and depositional sequences. In: Ross, C.A., Haman, D. (Eds.), Timing and Depositional History of Eustatic Sequences: Constraints on Seismic Stratigraphy. Cushman Foundation for Foraminiferal Research, Spec. Pub, vol. 4, pp. 137–149.

Roth, S., Reijmer, J.J.G., 2005. Holocene millennial to centennial carbonate cyclicity recorded in slope sediments of the Great Bahama Bank and its climatic implications. Sedimentologoy 52, 161–181.

Ruddiman, W.F., 2001. Earth's Climate Change: Past and Future. Freeman, New York. 465 pp.

Sandberg, C.A., Gutschick, R.C., 1980. Sedimentation and biostratigraphy of Osagean and Meramecian starved basin and foreslope, western United States. In: Fouch, T.D., Magathan, E. (Eds.), Paleozoic Paleogeography of West-central United States: Rocky Mountain Section. SEPM, West-central United States Paleogeography Symposium, vol. 1, pp. 129–147.

Sandberg, C.A., Zeigler, W., Dreesen, R., Butler, J.L., 1988. Late Fransian mass extinction: conodont event stratigraphy, global changes, and possible causes. Courier Forschungsinstitut Senckenberg 102, 263–307.

Sandberg, C.A., Poole, F.G., Johnson, J.G., 1989. Upper Devonian of the western United States. In: McMillan, N.J., Embry, A.F., Glass, D.J. (Eds.), Devonian of the World: Calgary. Canadian Society of Petroleum Geologists, Memoir, vol. 14, pp. 183–220.

Sando, W.J., 1985. Revised Mississippian time scale, western interior region, conterminous United States. U.S. Geological Survey Bulletin 1605-A, A15–A26.

Sakai, K., Peltier, W.R., 1997. Dansgaard–Oeschger oscillations in a coupled atmosphere–ocean climate model. Journal of Climate 10, 949–970.

Sarnthein, M., Kennett, J.P., Allen, J.R.M., Beer, J., Grootes, P., Laj, C., McManus, J., Ramesh, R., SCOR-IMAGES Working Group 117, 2002. Decadel-to-millennial scale climate variability—chronology and mechanism: summary and recommendations. Quaternary Science Reviews 21, 1121–1128.

Sarnthein, M., van Kreveld, S., Erlenkeuser, H., Grootes, P.M., Kucera, M., Pflaumann, U., Schulz, M., 2003. Centennial-to-millennial-scale periodicities of Holocene climate and sediment injections off the western Barents shelf, 75°N. Boreas 32, 447–461.

Schlager, W., 1993. Accommodation and supply—a dual control on stratigraphic Sequences. Sedimentary Geology 86, 111–136.

Schulz, M., 2002. On the 1470-year pacing of Dansgaard–Oeschger warm events. Paleoceanography 17. doi:10.1029/2000PA000571.

Schulz, M., Paul, A., 2002. Holocene climate variability on centennial-to-millennial time scales. 1. Internal feedbacks and external forcings as possible causes. In: Wefer, G., Hehre, W.H., Jansen, E. (Eds.), Climate Development and History of the North Atlantic Realm. Springer–Verlag, pp. 41–54.

Schulz, H., von Rad, U., Erlenkeuser, H., 1998. Correlations between Arabian Sea and Greenland climate oscillations of the past 110,000 years. Nature 393, 54–57.

Scotese, C.R., 2001. Paleomap Project. http://www.scotese.com/ July, 2001.

Steenbrink, J., Kloosterboer-van Hoeve, M.L., Hilgen, F.J., 2003. Millennial-scale climate variations recorded in Early Pliocene colour reflectance time series from the lacustrine Ptolemais Basin NW Greece. Global and Planetary Change 36, 47–75.

Stuiver, M., Braziunas, T.F., 1989. Atmospheric 14C and century scale solar oscillations. Nature 338, 405–408.

Suess, H.E., 1971. Climatic changes and the atmospheric radiocarbon level. Palaeogeography, Palaeoclimatology, Palaeoecology 10, 199–2002.

Svensmark, H., Friis-Christensen, E., 1997. Variation of cosmic ray flux and global cloud coverage—a missing link in solar–climate relationships. Journal of Atmospheric and Solar–Terrestrial Physics 59, 1225–1232.

Sweet, W.C., 2000. Conodonts and biostratigraphy of Upper Ordovician strata along a shelf to basin transect in central Nevada. Journal of Paleontology 74, 1148–1160.

Tada, R., Tomohiso, I., Itaru, K., 1999. Land–ocean linkages over orbital and millennial timescales recorded in late Quaternary sediments of the Japan Sea. Paleoceanography 14, 236–247.

Tappan, H., Loeblich Jr., A.R., 1973. Evolution of the oceanic plankton. Earth Science Reviews 9, 207–240.

Thouveny, N., de Beaulieu, J., Bonifay, E., Creer, K.M., Gulot, J., Icole, M., Johnsen, S., Jouzel, J., Reille, M., Williams, T., Williamson, D., 1994. Climate variations in Europe over the past 140 kyr deduced from rock magnetism. Nature 371, 503–506.

Tucker, R.D., Bradely, D.C., VerStraeten, C.A., Harris, A.G., Ebert, J.R., McCutcheon, S.R., 1998. New U–Pb zircon ages and the duration and division of Devonian time. Earth and Planetary Science Letters 158, 175–186.

Vail, P.R., Mitchum Jr., R.M., Thompson III, S., 1977. Seismic stratigraphy and global changes of sea level, 4. Global cycles of relative changes of sea level. American Association of Petroleum Geologists Memoir 26, 83–97.

Van Geel, B., Renssen, H., 1998. Abrupt climate change around 2650 BP in north-west Europe: evidence for climatological teleconnections and tentative explanation. In: Isaar, A., Brown, N. (Eds.), Water, Environment, and Society in Times of Climatic Change. Kluwer, Dordrecht.

Van Geel, B., Raspopov, O.M., Renssen, H., van der Plicht, J., Dergachev, V.A., Meijer, H.A.J., 1999. The role of solar forcing upon climate change. Quaternary Science Reviews 18, 331–338.

Van Kreveld, S.A., Sarnthein, M., Erlenkeuser, H., Grootes, P., Jung, S., Nadeau, M.J., Pflaumann, H., Voelker, A., 2000. Potential links between surging ice sheets, circulation changes, and the Dansgaard–Oeschger cycles in the Irminger Sea, 60–18 kyr. Paleoceanography 15, 425–442.

Walther, J.J., 2005. Essentials of Geochemistry. Jones and Bartlett Publishers, Sudbury, Ma. 704 pp.

Wang, Y.J., Cheng, H., Edwards, R.L., An, Z.S., Wu, J.Y., Shen, C.C., Dorale, J.A., 2001. A high-resolution absolute dated late Pleistocene monsoon record from Hulu Cave, China. Science 294, 2345–2348.

Westphal, H., Munnecke, A., 2003. Limestone–marl alternations: a warm-water phenomenon? Geology 31, 263–266.

Westphal, H., Head, M.J., Munnecke, A., 2000. Differential diagenesis of rhythmic limestone alternations supported by palynological evidence. Journal of Sedimentary Research 70, 715–725.

Westphal, H., Munnecke, A., Pross, J., Herrle, J.O., 2004. Multiproxy approach to understanding the origin of Cretaceous pelagic limestone–marl alternations (DSDP site 391, Blake–Bahama Basin). Sedimentology 51, 109–126.

Winton, M., 1997. The effect of cold climate upon North Atlantic Deep Water formation in a simple ocean–atmosphere model. Journal of Climate 10, 37–51.

Woillard, G.M., Mook, W.G., 1982. Carbon-14 dates at Grande Pile: correlation of land and sea chronologies. Science 215, 159–161.

Yiou, P., Genthon, C., Ghil, M., Jouzel, J., LeTrout, H., Barnola, J.M., Lorious, C., Korotkevitch, Y.N., 1991. High-frequency paleovariability in climate and CO2 levels from Vostok ice-core records. Journal of Geophysical Research 96, 365–378.

Young, G.C., Laurie, J.R. (Eds.), 1996. An Australian Phanerozoic Timescale, Melbourne. Oxford University Press.